Subantarctic mode water: Distribution and circulation

Article *in* Ocean Dynamics · November 2011

DOI: 10.1007/s10236-010-0352-9

2 authors:

Laura Herraiz-Borreguero
National Oceanography Centre, Southampton
19 PUBLICATIONS **430** CITATIONS

Stephen R. Rintoul
The Commonwealth Scientific and Industrial Research Organisation
204 PUBLICATIONS **11,639** CITATIONS

Ocean Dynamics
DOI 10.1007/s10236-010-0352-9

Subantarctic mode water: distribution and circulation

Laura Herraiz-Borreguero · Stephen Rich Rintoul

Received: 21 April 2010 / Accepted: 19 October 2010

Abstract The subduction and export of subantarctic mode water (SAMW) as part of the overturning circulation play an important role in global heat, freshwater, carbon and nutrient budgets. Here, the spatial distribution and export of SAMW is investigated using Argo profiles and a climatology. SAMW is identified by a dynamical tracer: a minimum in potential vorticity. We have found that SAMW consists of several modes with distinct properties in each oceanic basin. This conflicts with the previous view of SAMW as a continuous water mass that gradually cools and freshens to the east. The circulation paths of SAMW were determined using (modified) Montgomery streamlines on the density surfaces corresponding with potential vorticity minima. The distribution of the potential vorticity minima revealed "hotspots" where the different SAMW modes subduct north of the Subantarctic Front. The subducted SAMWs follow narrow export pathways into the subtropical gyres influenced by topography. The export of warmer, saltier modes in these "hotspots" contributes to the circumpolar evolution of mode water properties toward cooler, fresher and denser modes in the east.

Keywords Subantarctic mode water · Potential vorticity · Montgomery streamfunction · Circulation · Spatial distribution

Responsible Editor: Karen J. Heywood

L. Herraiz-Borreguero
Quantitative Marine Science Program, Institute of Marine and Antarctic Studies, University of Tasmania,
Hobart, Tasmania, Australia

L. Herraiz-Borreguero (✉)
Commonwealth Scientific and Industrial Research Organisation (CSIRO), Marine and Atmospheric Research,
Hobart, Tasmania, Australia
e-mail: lherraiz@utas.edu.au

S. R. Rintoul
Centre for Australian Weather and Climate Research—a partnership of the Bureau of Meteorology and Commonwealth Scientific and Industrial Research Organisation (CSIRO),
Hobart, Tasmania, Australia

S. R. Rintoul
Wealth from Oceans National Research Flagship,
CSIRO Marine and Atmospheric Research,
Hobart, Tasmania, Australia

L. Herraiz-Borreguero · S. R. Rintoul
Antarctic Climate and Ecosystems Cooperative Research Centre,
Hobart, Tasmania, Australia

1 Introduction

Subantarctic mode water (SAMW) was first identified and mapped as an homogeneous layer extending from near the surface to depths of more than 600 m on the equatorward side of the Subantartic Front (SAF) (McCartney 1977, 1982). McCartney (1977) introduced the idea that SAMW properties reflect the southward spiralling of the SAF, becoming progressively denser and cooler from the southwest Atlantic Ocean (SAMW temperature, ~15°C) to the southeast Pacific Ocean (4–5°C; Fig. 1, from McCartney 1977). McCartney (1977) concluded that the downstream evolution of SAMW properties likely reflects gradual modification by air–sea fluxes. However, the circumpolar continuity of the SAMW along the equatorward side of the SAF is not yet clear.

Different forcing mechanisms drive the formation of SAMW in the Subantarctic Zone (SAZ). The SAZ is the region delimited by the Subtropical Front and the Subantarctic Front. Ekman pumping in the SAZ favours the formation of deep-mixed layers associated with SAMW. Moreover, the combined effect of air–sea fluxes and Ekman transport mainly drive SAMW formation (e.g., McCartney 1977; Sloyan and Rintoul 2001; Rintoul and England 2002). Eddy heat diffusion modifies their effects, causing local cooling or warming of SAMW (Sallèe et al. 2008).

Published online: 11 November 2010

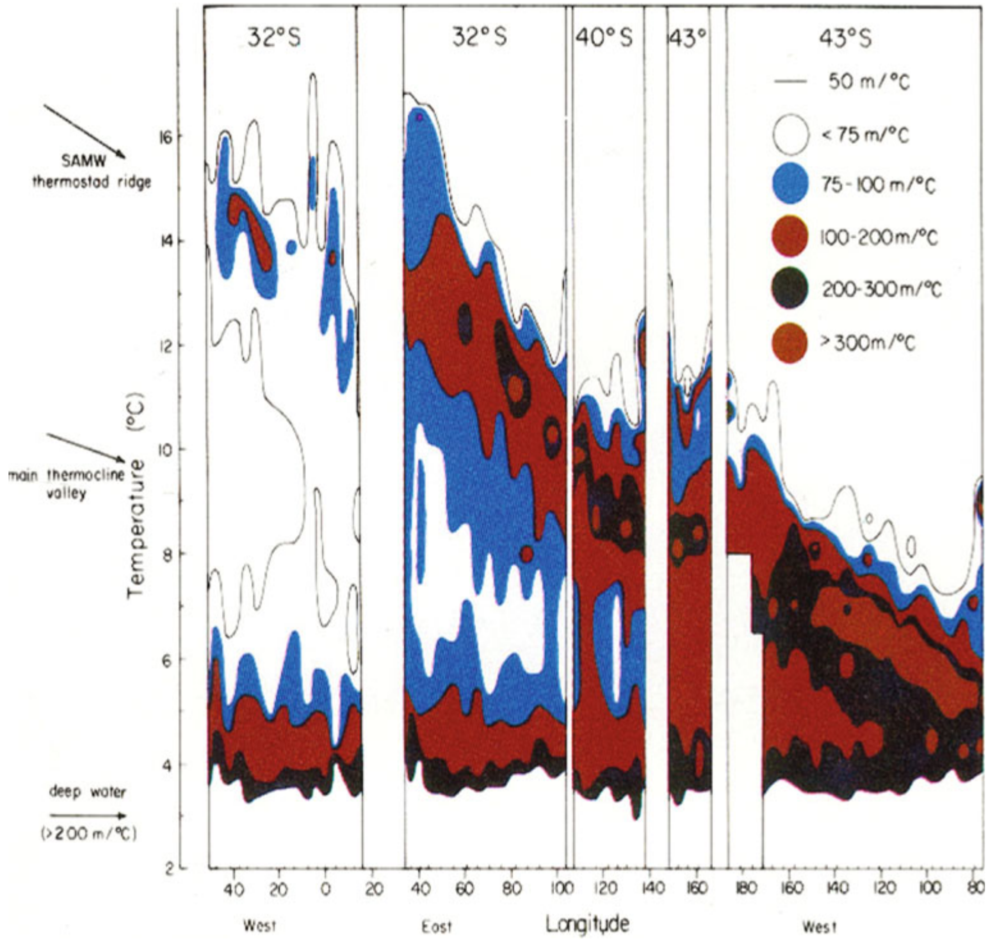

Fig. 1 SAMW thermostad strength as a function of temperature and longitude. The SAMW thermostad runs from the 14–15°C in the western Atlantic through 8–9°C (South of Australia, 120° E) and ending at 5°C in the eastern Pacific (McCartney 1977)

Two Mode Waters have been described in the southwestern Atlantic Ocean. The cold and fresh SAMW that crosses Drake Passage from the southeastern Pacific Ocean is the densest of the two varieties. In its northward flow following the Malvinas Current, west of 60° W, it encounters lighter waters and progressively sinks to occupy 800–1,000 m depths (McCartney 1977). The warmer and saltier SAMW variety is found at the surface, in the Brazil–Malvinas Confluence. The Subtropical Mode Water can be split into two variants separated by the eastward extensions of the Brazil Current Front at approximately 42° W (Roden 1986; Tsuchiya et al. 1994), and they are confined to the region west of 25° W and south of 20° S. The high spatial variability of the SAF, mainly due to effects of bathymetry on the flow and the confluence of the Brazil and Malvinas Currents, make the southwest Atlantic one of the regions with highest eddy kinetic energy of the world ocean (De Miranda et al. 1999; Scharffenberg and Stammer 2010). As a result, several definitions and locations of the warm SAMW and Subtropical Mode Water have been given due partly to their close proximity in this region (e.g., McCartney 1977, 1982; Tsuchiya et al. 1994; Provost et al. 1995; Mémery et al. 2000).

Two varieties of SAMW have been described in the south Indian Ocean. The western side of the Indian Ocean holds the lighter and lower volume of the two varieties (McCartney 1982; Hanawa and Talley 2001). The Kerguelen Plateau (70–80° E) represents the boundary between the two varieties, with significantly higher oxygen saturation in the mixed layer on the eastern side of the Plateau (Talley 1999). McCarthy and Talley (1999) found a layer of low potential vorticity centred at 90° E–40° S which they interpreted as a signature of deep-mixed layers, from the southern Indian Ocean, formed by convection, subducted and advected toward the subtropics in agreement with McCartney's work (1982) and CFC concentrations (Fine 1993; Fine et al. 2008). The combination of several factors (e.g., convergence of two deep-reaching fronts with an energetic eddy field resulting from flow interactions with bathymetry, strong cooling due by eddy diffusion, Ekman heat transport, and a circumpolar maximum in the mean wind field) make the region downstream of the Kerguelen Plateau the dominant source of SAMW in the Indian Ocean (Sallèe et al. 2006).

As in the Indian Ocean, the properties and circulation of SAMW in the south Pacific differ from west to east. The lightest Pacific SAMW is restricted to the southwest Pacific, south of 35° S (McCartney and Baringer 1993; Sokolov and Rintoul 2000). The southeastern Pacific SAMW is the densest of the Pacific SAMWs and has a close relationship with Antarctic Intermediate Water (AAIW). This dense SAMW is exported along two paths: through Drake Passage into the Atlantic Ocean and into the subtropical gyre of the south Pacific Ocean (McCartney 1977, 1982). The close relationship between SAMW and AAIW in the southeastern Pacific is still under debate. Early studies claim SAMW is the precursor of AAIW, an intermediate water mass coincident with a salinity minimum (e.g., McCartney 1977; Talley 1996; Hanawa and Talley 2001). On the other hand, the fact that interannual variability of AAIW was independent from that of SAMW has been interpreted as evidence that AAIW is supplied by Antarctic Surface Water (Naveira-Garabato et al. 2009).

To identify SAMW in the formation and subduction regions and describe its circulation paths, we use potential vorticity as a tracer. Section 2 describes the data and methods used. Section 3 shows the distribution of SAMW and subduction regions, followed by a discussion on SAMW modes and circulation. Finally, Section 4 summarises our major findings.

2 Data and methods

Since 2000, the ocean has been populated with temperature/salinity profiling floats, known as Argo.[1] Argo floats are deployed in ice-free oceans, profiling temperature/salinity in the upper ocean to depths up to 2,000 m. Data are made freely available by the International Argo Project and the national programmes that contribute to it. This study used profiles, mainly covering from 2005 to 2008, that passed the Argo real-time quality control flag 1, with data on their position, date, temperature and salinity from 10 to 1,800 m.

The Argo float programme provides an extensive dataset of the ocean, especially of the Southern Ocean and the south Pacific Ocean where vast areas have been poorly sampled in the past. We are confident about the quality of the data for our study despite the reported pressure sensor drifts (Barker et al. 2010), as these errors are found on few floats in the Southern Ocean and also, the pressure drifts affect mainly the accuracy of ocean heat content and sea level budget measurements, not calculated in this study. The spatial coverage provided by Argo is excellent compared to historical data; however, some regions are not well sampled and only a short time period is covered. The CSIRO Climatological Atlas for Regional Seas (CARS 2006a/2009)[2] complements the Argo data in this regard.

CARS2006a is an atlas of seasonal ocean water properties, covering the entire southern hemisphere and equatorial regions in which temperature, salinity, oxygen, nitrate, silicate and phosphate are mapped (Ridgway et al. 2002; Dunn and Ridgway 2002). It comprises mean fields and average seasonal cycles, derived from all available historical subsurface ocean property measurements mostly collected from the last 50 years (primarily research vessel instrument casts and autonomous profiling floats). The vertical and spatial resolution of CARS2006a used here is 10 m and half a degree, respectively. Temperature and salinity units are degree Celcius and the Practical Salinity Scale 1978 (PSS-78).

SAMW is produced by deep convection in winter, forming thick homogeneous layers that are rich in oxygen. These properties can be used to trace the spreading paths of mode waters after they leave the surface, as the characteristic properties are retained for great distances. Mode waters stand out from the surrounding water masses as a potential vorticity minimum layer (minimum in hydrostatic stability). Potential vorticity (PV) is conservative (away from source and mixing regions) and hence, provides an excellent tracer for mode water (McCartney 1982). PV plays an important role in large–scale oceanography, acting both passively as a tracer and dynamically to direct the flow. Potential vorticity is given by:

$$\mathrm{PV} = \frac{(f + \xi)}{\rho} \frac{d\rho}{dz},$$

where f is the planetary vorticity, ξ is the relative vorticity, $(v_x–u_y)$ and $\frac{1}{\rho}\frac{d\rho}{dz}$ is the stretching term. The relative vorticity is negligible in comparison to the other two terms in large-scale studies, where the Rossby number is small, except in strong boundary currents. And so, we will refer to potential vorticity as the quantity

$$\mathrm{PV} = \frac{f}{\rho} \frac{d\rho}{dz}.$$

We evaluate PV over a 50-m depth interval using simple differences. For first and last 50 m of the density profile, forward and backward differences were taken. No depth cut-off has been made prior to the calculation of the PV.

The geostrophic circulation transporting SAMW from the formation regions is analysed on neutral density surfaces using an improved Montgomery geostrophic streamfunction (Montgomery 1937; McDougall 1989; Zhang and Hogg 1992) by using a reference point on the

[1] http://www.marine.csiro.au/~sal119/Argo.html; http://www.ifremer.fr/coriolis/cdc/argo.htm

[2] http://www.marine.csiro.au/~dunn/cars2009/

isopycnal surface in question (McDougal and Klocker 2010). γ^n is the neutral density (kgm^{-3}) variable of Jackett and McDougall (1997). The geostrophic streamfunction in approximately neutral surfaces is expressed as

$$M = \frac{1}{2}(p-\widehat{p})\widehat{\delta}\left(\widehat{S},\widehat{\Theta},\widehat{p}\right) - \frac{1}{12}\frac{T_b^{\Theta}}{\rho}\left(\Theta-\widehat{\Theta}\right)(p-\widehat{p})^2 - \int_0^p \widehat{\delta}dp$$

where p represents the depth of the isopycnal surface and varies spatially, and

$$\widehat{\delta} = \frac{1}{\rho(S,T,p)} - \frac{1}{\rho\left(\widehat{S},\widehat{\Theta},\widehat{p}\right)}$$

where $\rho(S, T, p)$ represents the in situ density; $\rho\left(\widehat{S},\widehat{\Theta},\widehat{p}\right)$ is a reference density for the isopycnal surface (neutral density) with $\widehat{S}$, $\widehat{\Theta}$ and $\widehat{p}$ as the median values on that surface and, T_b^{Θ} is the thermobaric coefficient (note that $T_b^{\Theta}\rho^{-1} \approx 2.7\times10^{-15}\mathrm{K}^{-1}(\mathrm{Pa})^{-2}\mathrm{m}^2\mathrm{s}^{-2}$). Note that the Montgomery streamfunction is an approximation and no exact streamlines on isopycnals exist. The circulation analysed in this work corresponds to the baroclinic mode. Factors such as the assumption of a 1,800-m level of no motion could impact on the representativeness of the Montgomery streamfunction in portraying the actual circulation throughout the study region (especially in the ACC or other regions of strong currents).

The properties of the SAMW in the Southern Ocean and away from the formation areas are examined as follows. SAMW was defined as a PV minimum between [0, 1.5×10^{-9}] m^{-1}s^{-1}. The distribution of PV on neutral density surfaces is used to select the density surface that best represents the pycnostad layer in each oceanic basin. The properties of SAMW on each γ^n surface are described next, as well as the export paths to the subtropics inferred from the (modified) Montgomery streamfunction. Temperature and salinity on isopycnal surfaces are only shown for the SAMW core PV minimum range, denoted by values of PV≤1×10^{-9} m^{-1}s^{-1} and below 200 m. This depth cut-off is used to reduce the seasonal signal at the top of the water column. The main bathymetry features of the Indian and Pacific Oceans are shown in Fig. 3 as a reference.

3 Distribution of subantarctic mode water

3.1 Circumpolar distribution

The annual representation of CARS2006a temperature and salinity was used to calculate the potential vorticity as a means to identify SAMW. SAMW forms a uniform pool of low PV in the neutral density (kgm^{-3}) range 27.1 to 27.2 kgm^{-3} west of Drake Passage at 55° S (Fig. 2f). East of Drake Passage, a denser SAMW (γ^n=27.2–27.3 kgm^{-3}) enters the south Atlantic Ocean. Its track is rapidly lost east of 320° E. Further north at 50° S, SAMW occupies most of the south Pacific Ocean, extending from west of New Zealand (~180° E) to South America (Fig. 2b–e). At this latitude, SAMW is also seen in the Indian Ocean, southwest of New Zealand (~160° E), increasing its longitudinal extention eastward at lower latitudes. Note that the Pacific and Indian SAMW pools can be traced up to 25° S, and they appear as two independent features at all latitudes.

At a first glance, SAMW is seen as a uniform "pool" whose density, uniformity and depth vary spatially; however, closer inspection reveals the distinct modes that form SAMW circumpolarly. A common feature seen in the SAMW pool is the "stacking" of modes of different density (kgm^{-3}) in most latitudinal sections. In the Indian sector, three main γ^n ranges form the SAMW pool:

- 26.7≤γ^n≤26.8 (at 40° S, Fig. 2c)
- 26.8≤γ^n≤26.9 (from 40° to 25° S, Fig. 2a–c)
- 26.9≤γ^n≤27.0 (from 50° to 25° S, Fig. 2a–f)

In the south Pacific and south Atlantic sectors, SAMW is formed by denser modes:

- 27.0≤γ^n≤27.1 (from 50° to 35° S, Fig. 2b–e)
- 27.1≤γ^n≤27.2 (from 50° to 35° S, Fig. 2b–e)
- 27.2≤γ^n≤27.3 (at 55° S, Fig. 2f)

In each basin, lighter modes are restricted to the south west. Denser modes, originating in the south east, travel further north, especially in the Indian Ocean.

3.2 SAMW in the south Indian Ocean

The PV minimum (PV≤1.5×10^{-9} m^{-1}s^{-1}) spans a range of 26.75≤γ^n≤26.97 kgm^{-3} in neutral density, extending across most of the south Indian Ocean Basin (~40° to 170° E). A relatively light SAMW type with a density range of 26.75≤γ^n≤26.85 kgm^{-3} is found in the western side of the south Indian Basin, between ~70° and 90° E. A slightly denser SAMW type, 26.85≤γ^n≤26.97 kgm^{-3}, is found south of Australia between 120° and 170° E. It is also the most homogeneous SAMW with a PV minimum lower than 1×10^{-9} m^{-1}s^{-1}. SAMW properties and circulation paths are next described on two isopycnal surfaces, 26.8≤γ^n≤26.9 kgm^{-3}, corresponding to these two modes. A third mode will be described here for several reasons: its high pycnostad strength compared to the other Indian modes and also because it reaches the south Pacific Ocean.

Fig. 2 Annual mean potential vorticity (PV) as a function of depth and longitude (°E) at 55° S (**f**), 50° S (**e**), 45° S (**d**), 40°S (**c**), 35° S (**b**) and 25° S (**a**). Data taken from CARS Climatological Atlas for Regional Seas (CARS2006a). *White lines* depict neutral density isopycnals. *Grey stars* in the *x*-axes show the extent of the Atlantic, Indian and Pacific Oceans

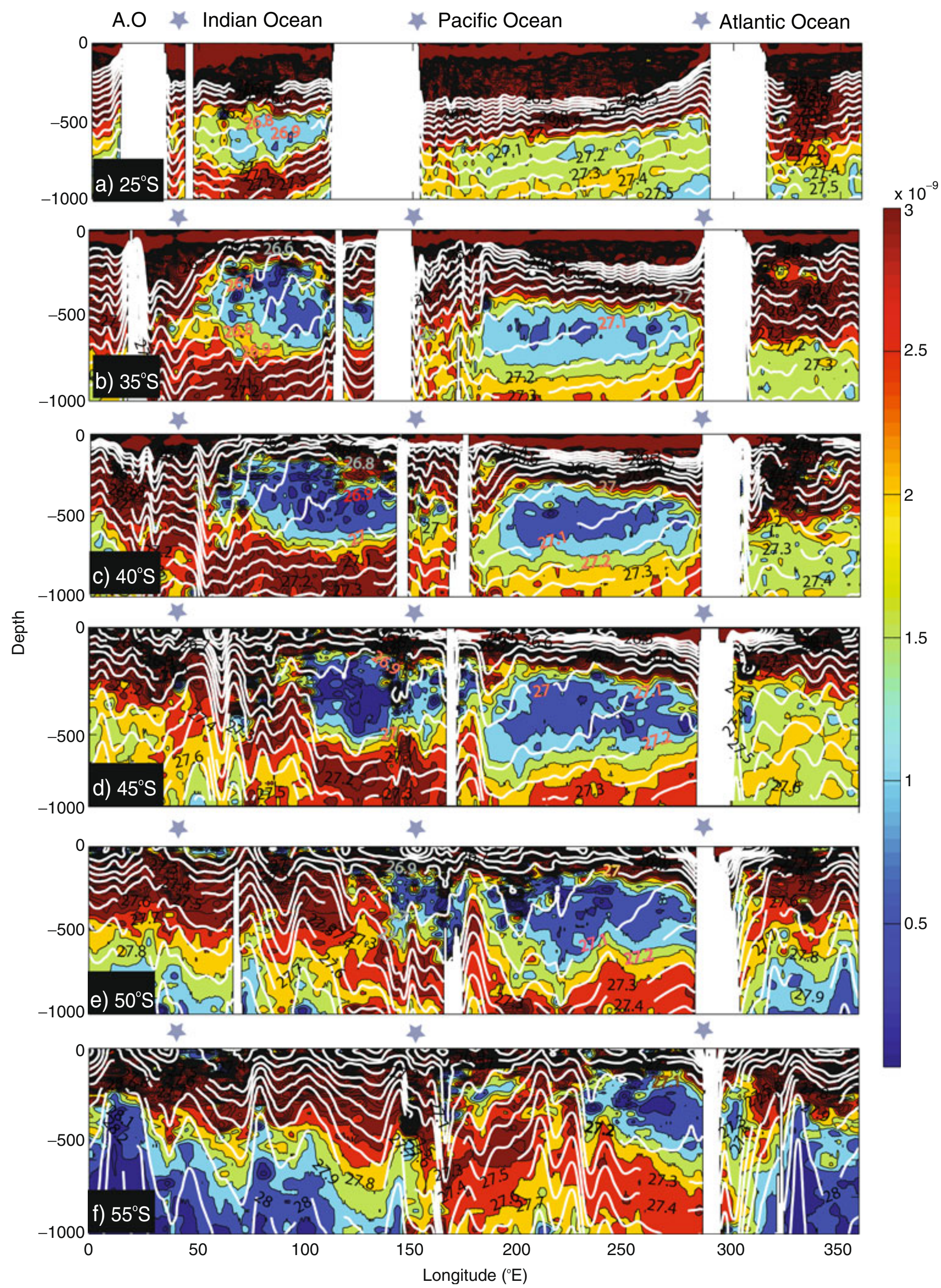

3.2.1 SAMW on γ^n= 26.8

Potential vorticity on the 26.8–γ^n surface reveals a tongue-like distribution of the light Indian SAMW (Fig. 4a). The low PV enters the basin through a narrow region between 80° and 100° E, south of 30° S, bounded in the west and south by the Southeast Indian Ridge and, in the northeast, by the Broken Plateau (Fig. 3). The lowest PV minimum (strongest SAMW pycnostad) lies just south of the STF (80°–100° E) where the anticyclonic circulation turns to the north. The streamline enclosing the SAMW "pool", hereafter $\Psi_{26.8}$ (Fig. 4, black contour), will be used as a reference to discuss the spatial variations of SAMW. Similar nomenclature is used in the following sections with the corresponding isopycnal subscript,$\Psi^i_{\gamma^n}$, where i is the number of streamlines used and γ^n is the isopycnal surface we are focused on.

The PV minimum spreads northwestward along $\Psi_{26.8}$ over a wider region after passing through the passage between the Southeast Indian Ridge and the Broken Plateau (~30° S, 80°–90° E; Fig. 3), reaching as far north as 20°–25°S before its signal vanishes. North of this passage, the erosion of the PV minimum is enhanced as it spreads along $\Psi_{26.8}$. The region of low PV is limited by a sharp boundary between the PV minimum and the high PV waters east of 100° E.

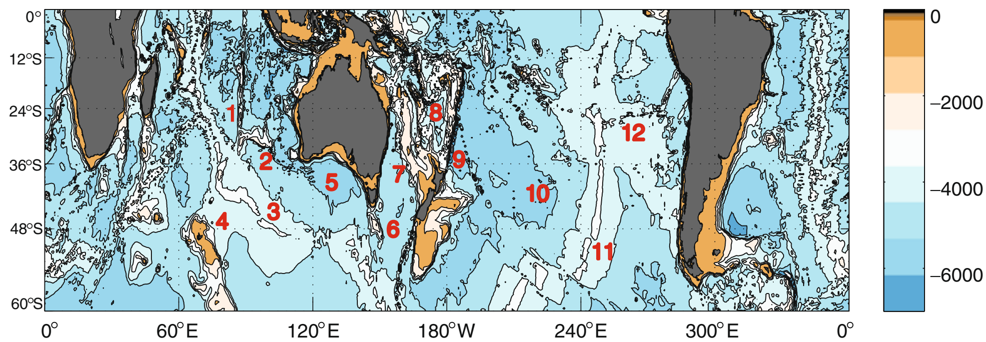

Fig. 3 Ocean topography in the south Indian and Pacific Oceans. *1* Ninetyeast Ridge; *2* Broken Plateau; *3* Southern Indian Ridge; *4* Kerguelen Plateau; *5* great Australian Bight; *6* South Tasman Rise; *7* Tasman Basin; *8* South Fiji Basin; *9* South Kermadec Ridge; *10* Southwest Pacific Basin; *11* East Pacific Rise; *12* Nazca Ridge

SAMW properties on γ^n=26.8 kgm^{-3} increase in a series of steps. SAMW has a temperature of 10–10.5°C and a salinity of 34.7–34.8 in the SAZ and increases up to ~1.2°C and 0.3, respectively, during its transit to the northern-most extent in the northwestern south Indian Basin. This transition to warmer and saltier waters occurs in a series of steps, coincident with bathymetric features. Temperature and salinity increase by up to 0.5°C and 0.1, respectively, north of the STF. South of the Southeast Indian Ridge and the Broken Plateau, SAMW temperature and salinity remain constant along $\Psi_{26.8.}$ SAMW properties change while transiting the passage between these two bathymetric features, entering the central south Indian Basin where, like PV, temperature and salinity change very slowly until the PV minimum has been completely eroded.

3.2.2 SAMW on γ^n= 26.9

The SAMW PV minimum on the 26.9–γ^n surface enters the subtropical indian gyre along two paths. The minimum PV is found between 95° and 120° E, just north of the SAF and along the $\Psi^1_{26.9}$ and $\Psi^2_{26.9}$ streamlines (Fig. 5a, black bold lines). The low PV enters the gyre from the east in a narrow range of Ψ. The 26.9–γ^n SAMW circulation splits southeast of the Broken Plateau (30° S, west of 100° E) and enters the central Indian Ocean following two paths. (1) SAMW follows the $\Psi^1_{26.9}$ streamline northward along the western Australian coast, east of the Broken Plateau. Between 20° and 25° S, SAMW flows westwards toward Madagascar where the PV minimum is eroded very quickly (following $\Psi^1_{26.9}$). The Indonesian Throughflow region acts as a high PV boundary at ~15° S. East of Madagascar, there is evidence of an exchange of waters with high PV moving slightly southward along the coast of Madagascar and northward, further east. (2) SAMW flows northwestward west of the Broken Plateau along $\Psi^2_{26.9}$. As seen on the γ^n= 26.8 kgm^{-3} surface, the low PV signature is eroded by mixing before the SAMW reaches the western side of the basin. There is no evidence of low PV water returning south in the western boundary, where high PV occupies the western gyre.

SAMW temperature and salinity on the 26.9–γ^n surface also show step-like changes linked to the encounter of SAMW with bathymetric features. Properties will be discussed following the two paths described above, starting from the Subantarctic Zone, where the lowest PV signature is found. The coldest and freshest (8.6–9°C and 34.55–34.65) SAMW is found north of the SAF (Fig. 5b, c). The transition to warmer and saltier SAMW occurs in a series of steps, coincident with bathymetry features, as seen on the 26.8–γ^n surface. Temperature and salinity increase 0.4°C and 0.05, respectively, (compared to values south of Australia) between 100° and 120° E. SAMW properties increase 0.2°C and 0.05 near the Broken Plateau. North and northwest of the Broken Plateau, SAMW temperature has increased by 1–1.5°C at 20° S (compared to Subantarctic Zone values). South of Australia and surrounding Tasmania, SAMW temperature and salinity increase from 8.6–9°C to 9.8–10°C (~1.2°C) and from 34.55–34.65 to 34.8–34.85 (~0.35; Fig. 5b, c). Differences in the regional circulation explain the erosion of the PV around Tasmania. Warm and salty waters carried by the remnant East Australian Current, in the form of isolated eddies, mix with waters from the SAZ (better seen in the higher salinity surrounding Tasmania in Fig. 5c).

The changes in SAMW properties along the export pathway can be more clearly seen in plots of temperature and salinity anomalies (relative to the mean properties along $\Psi^2_{26.9}$) along approximate streamlines (Fig. 6). East of 110° E, the PV minimum cools and freshens as it approaches the south Tasman Rise (“stations” 2 and 3, Fig. 6b). South of Tasmania, SAMW properties increase over 1°C between “stations” 3 and 4, reflecting the high influence of the advection of warm and salty subtropical waters from the Tasman Sea (Herraiz-Borreguero and Rintoul 2010). South of the Broken Plateau (30°–35° S and 100°–120° E), between “stations” 5 and 6, mean properties are constant (error bars show the standard deviation per “station”). At “station” 6, temperature, salinity and PV decrease likely reflecting the close location to the pathway the subducted 26.9–γ^n and 26.9–γ^n SAMW modes follow in the interior (see Section 4). West of the Broken Plateau (~ “station” 6), at 100° E, a rapid increase

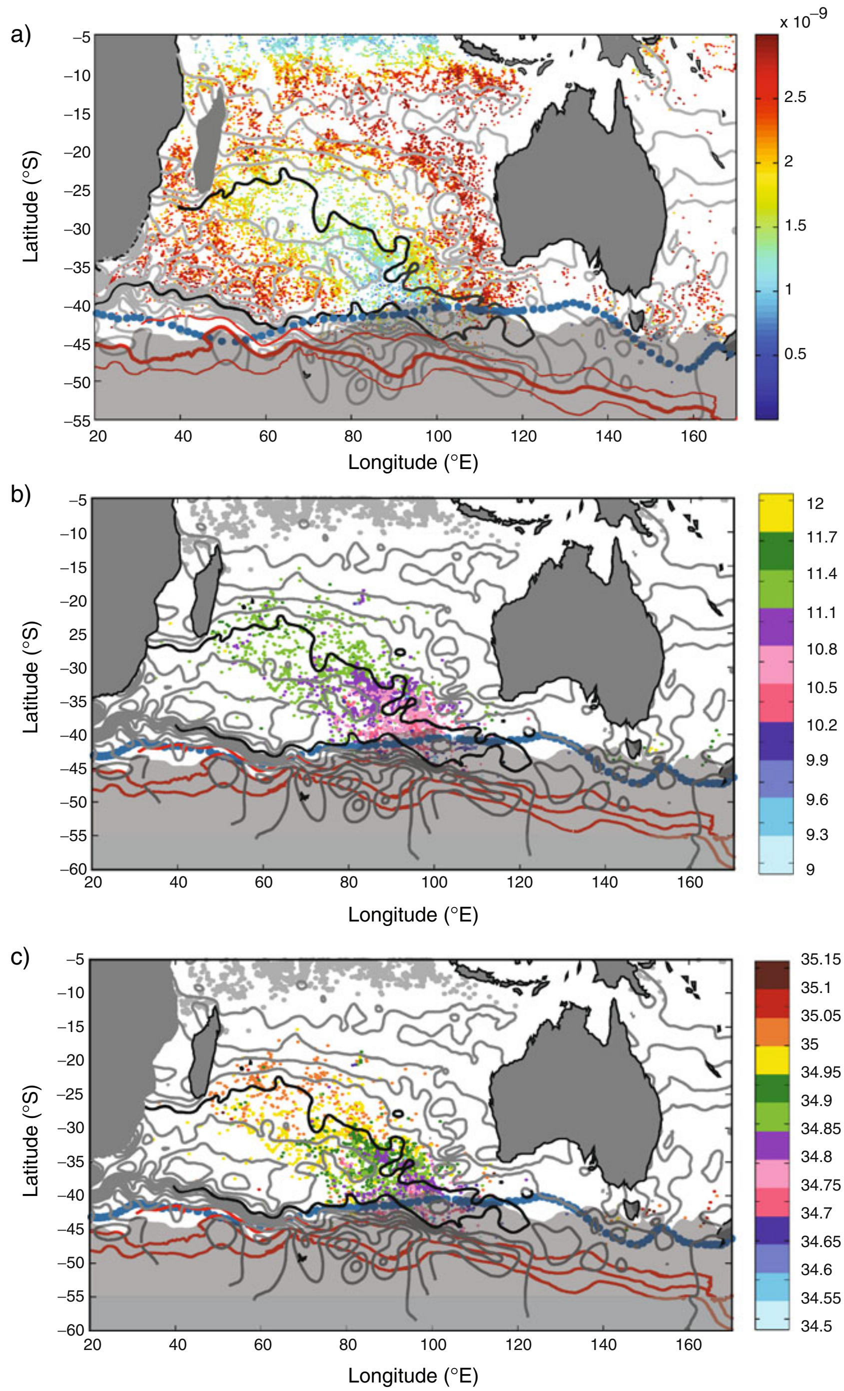

Fig. 4 Distribution of SAMW on the 26.8–γ^n surface. **a** Potential vorticity, **b** temperature and **c** salinity of the SAMW, where SAMW is identified as PV≤1.5×10^{-9} $m^{-1}s^{-1}$. Modified montgomery streamlines are depicted by *grey lines*. The area south of this neutral density surface outcrop has been masked by a *grey* surface to mark regions where the streamlines loose accuracy. $\Psi_{26.8}$, the streamline that best represents the SAMW flow, is highlighted a *thick black line*. *Blue dotted* and *red lines* depict the subtropical front and the subantarctic front, respectively. Note that the front positions were calculated using different techniques, and they overlap at some locations. Each *dot* represents an Argo profile

in SAMW temperature and salinity is followed by the erosion of the PV minima towards "station" 7 as SAMW flows over rough topography (Fig. 6c).

3.2.3 SAMW on γ^n= 26.94

The streamlines and PV spatial distribution on γ^n= 26.94 kgm^{-3} show similarities with the 26.9–γ^n SAMW (Figs. 5 and 7); however, the low PV is much more restricted to the great Australian Bight. The two pathways (northward along the western Australia coast, and west to south of the Broken Plateau) observed on the 26.9–γ^n surface are also seen on this density surface. Note that there is a "gap" with no floats north/northwest of the Broken Plateau on both 26.9–γ^n and 26.94–γ^n surfaces. The SAMW PV minimum signal on the 26.94–γ^n surface is found south of Tasmania and on either side of New Zealand (Fig. 7). SAMW temperature and salinity cools

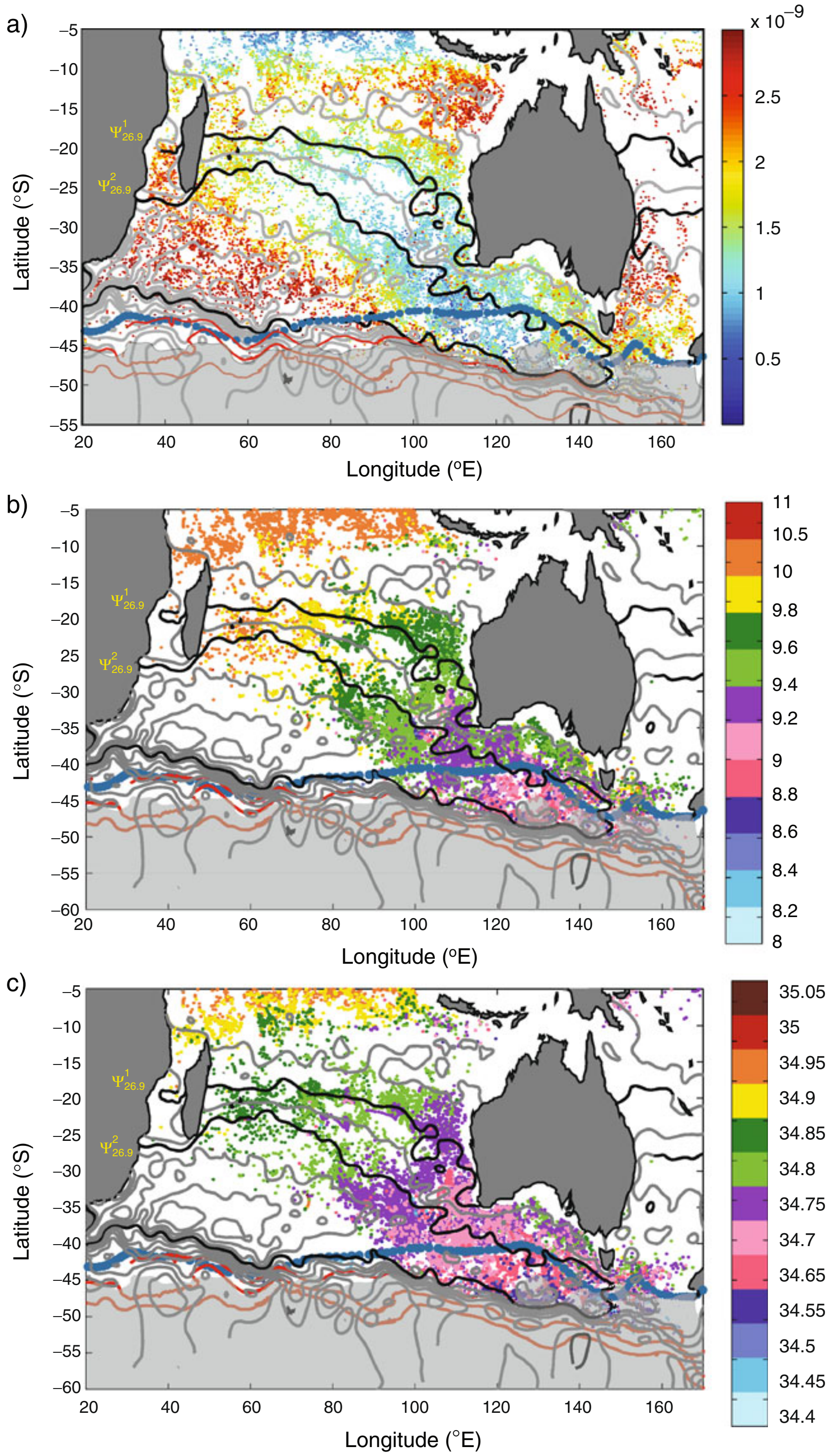

Fig. 5 Distribution of SAMW on the 26.9–γ^n surface. Details follow Fig. 4. The $\Psi^1_{26.9}$ and $\Psi^2_{26.9}$streamlines are shown as a thick *black line*

and freshens eastward (not shown) from southwest to southeast of Tasmania (0.2°C; 0.1), and shows similar temperature and salinity values (8.4–8.6°C; 34.5–34.6) on either side of New Zealand. South east of New Zealand, a cluster of SAMW is found at the turning point of an anticyclonic circulation (40°–50° S, 200°–210° E).

3.3 SAMW in the South Pacific Ocean

Low PV is found in a neutral density range of $27.0\leq\gamma^n<27.2$ kgm^{-3} in the south Pacific Ocean. The lightest SAMW is found west of New Zealand. West of 240° E, the PV minimum of the SAMW coincides with a density of

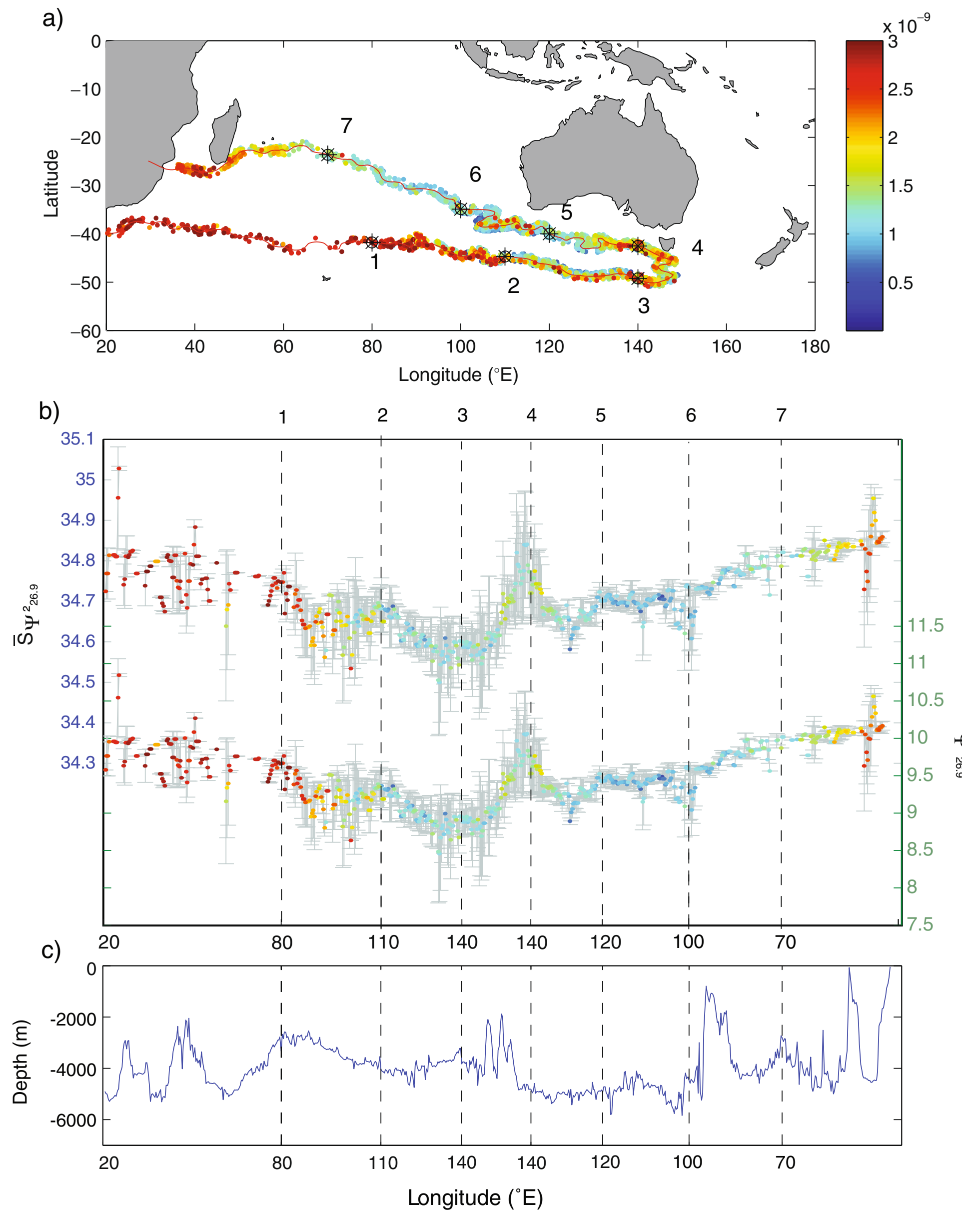

Fig. 6 Temperature and salinity changes along $\Psi^2_{26.9}$. **a** Colour-coded dots (according to the Potential vorticity) are Argo floats within 100 km from $\Psi^2_{26.9}$ (in *red*). *Black stars* were placed to mark the eastward temperature and salinity anomaly changes along $\Psi^2_{26.9}$. **b** Temperature and salinity anomaly along $\Psi^2_{26.9}$. *Grey bars* denote the standard deviation. Each *dot* is the mean within a 100-km radius for every position in the streamline. *Vertical black dashed lines* indicate the position of the *black stars* in (**a**). **c** Ocean bathymetry along $\Psi^2_{26.9}$

27.05 kgm^{-3}, with the minimum PV observed between 220° and 240° E. East of 240° E, SAMW becomes progressively denser as it approaches the South American continent. The lowest PV values are located at 260° and 280° E. The SAMW properties are next described on four isopycnal surfaces, 27.0≤γ^n≤27.05 kgm^{-3} and, 27.1≤γ^n≤ 27.15 kgm^{-3}. We have chosen to group the density surfaces in two ranges according to their position regarding the East Pacific Rise (Fig. 3; discussed in Section 5).

3.3.1 SAMW on 27.0–27.05

SAMW on the γ^n=27.0 kgm^{-3} surface occupies the southwest Pacific between the SAF in the south and a northern limit of ~30°–35° S (Fig. 8). The SAMW pycnostad strengthens eastward along the SAF, east of New Zealand, and turns northwestward at 230°–250° E, just west of the East Pacific Rise (Figs. 3, 8a and 9a). While the spatial distribution of the SAMW on the 27.0–γ^n and 27.05–γ^n surfaces show similarities (i.e. they are constrained to the southwest Pacific Basin—note that high PV is seen in the eastern basin on these isopycnals), the extent of the PV minimum and so, the ventilation efficiency, differ. The lightest SAMW (γ^n=27.0 kgm^{-3}) is found inside the subtropical gyre, east of New Zealand, between 35°–50° S and 180°–240° E (Fig. 8a). Two streamlines, Ψ^1_{27} and Ψ^2_{27}, delimit the narrow zone where the 27.0–γ^n SAMW enters the gyre (black bold lines; Fig. 8a). The 27.05–γ^n SAMW exceeds the lighter SAMW in spatial extent and pycnostad strength (Fig. 9a). It also

Fig. 7 Potential vorticity on the 26.94–γ^n surface, in the Indian sector (**a**) and in the Pacific sector (**b**) of the Southern Ocean. SAMW is identified as $PV \le 1.5\times10^{-9}\ m^{-1}s^{-1}$. Modified montgomery streamlines are depicted by *grey lines*. *Blue dotted* and *red lines* depict the subtropical front and the sub-antarctic front, respectively. Each *dot* represents an Argo profile

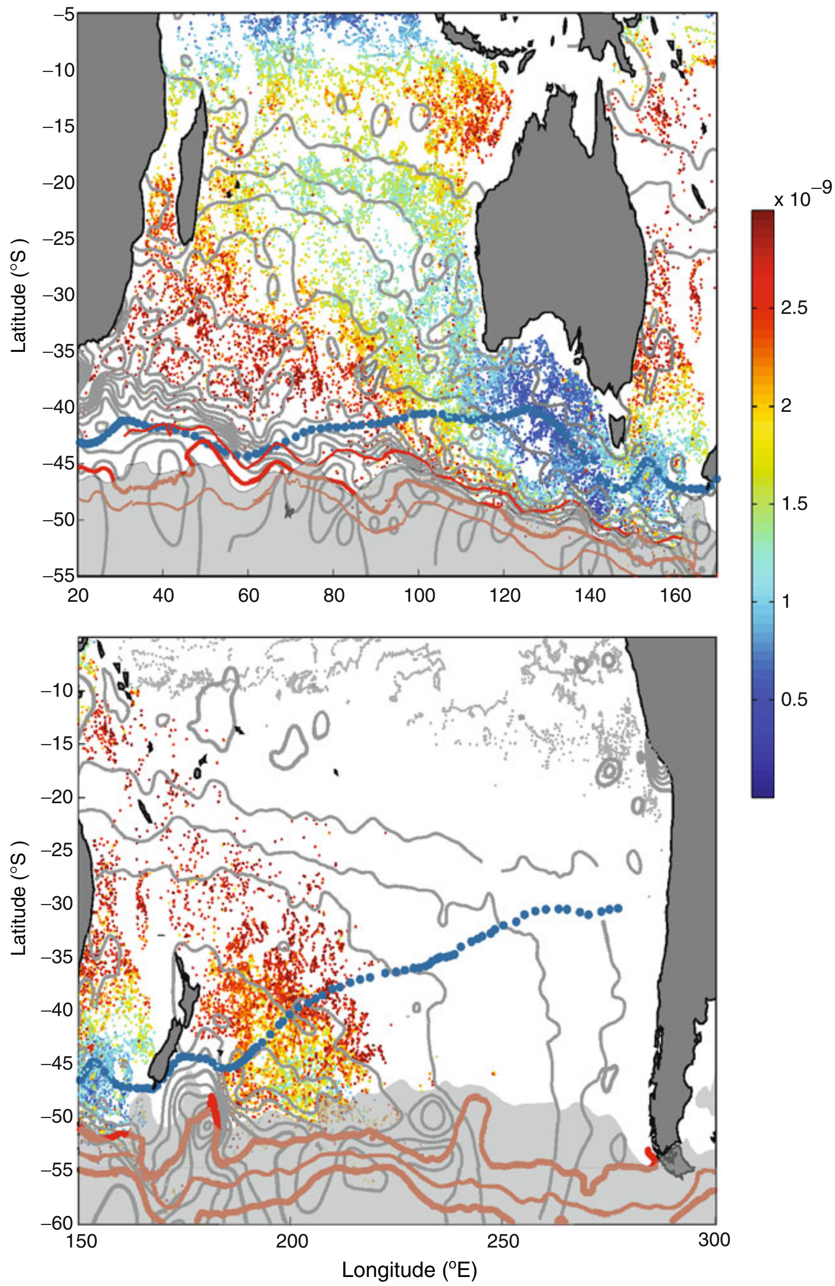

enters the subtropical gyre through a broader window west of the East Pacific Rise.

No evidence of PV minimum water entering the Tasman Sea is seen on these density levels. The signature of the 27.0–γ^n SAMW PV minimum erodes abruptly between the South Fiji Basin and New Zealand (30°–35° S, 180° E). Similar erosion occurs to the 27.05–γ^n SAMW whose core reaches 30° S before eroding completely south of the Polynesia (Figs. 8a, and 9a).

SAMW temperature and salinity increase anti–clockwise along streamlines on both density surfaces. The 27.0–γ^n SAMW mean temperature and salinity are 7.5°C and 34.4, respectively (Fig. 8b, c). The restricted extent of the 27.0–γ^n SAMW is reflected in the low variability of temperature and salinity with higher values northeast of New Zealand (7.8°C, 34.45), and lower values in the eastern part of the SAMW pool (34.35).

The 27.05–γ^n SAMW properties gradually change as it flows northwestward (Fig. 9b, c). The coldest and freshest 27.05–γ^n SAMW patch (6.2–6.6°C, 34.2–34.3) is found along the ACC (50°–55° S) and at the eastern part of the SAMW pool (55°–35° S, 220°–260° E) where the Mode Water enters the main thermocline in the subtropical gyre. The temperature and salinity of the 27.05–γ^n SAMW increase by 0.4–0.8°C and 0.15, respectively, as it flows to the west, away from the subduction area.

Fig. 8 Distribution of SAMW on the 27.0–γ^n surface. Details follow Fig. 4

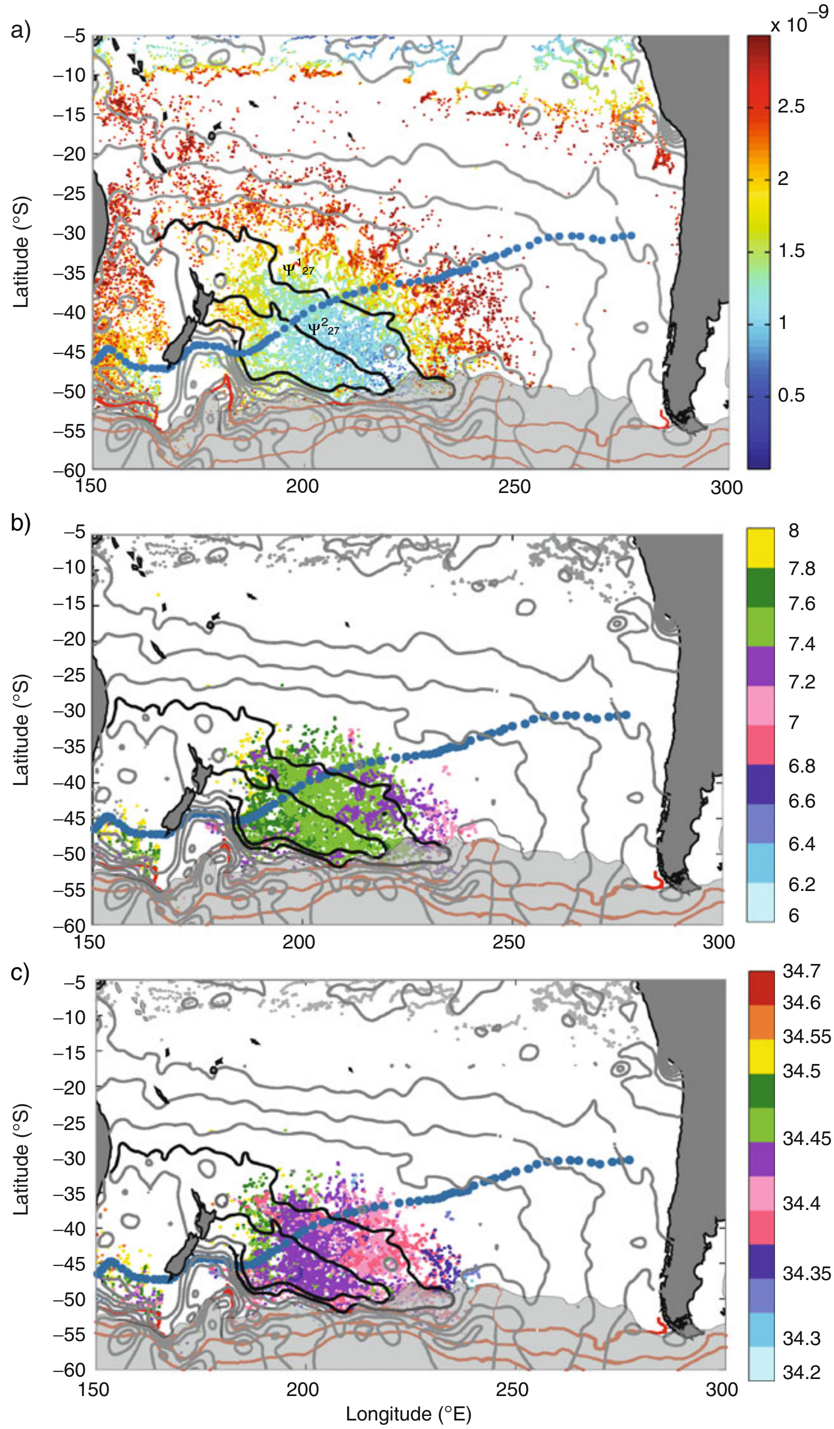

An example of the along-stream temperature and salinity change on γ^n=27.05 kgm^{-3} is shown in Fig. 10. The coldest and freshest SAMW (Fig. 10b) is found north of the SAF where the 27.05–γ^n SAMW reaches its eastern–most point (Fig. 9). Compared to the Indian Ocean where the topography is more complex, the pycnostad properties are stable over the smooth topography of the southeast Pacific. The lack of erosion of the low PV signal suggests very weak mixing, until the SAMW encounters the very steep ocean topography northeast of New Zealand, the South Kermadec Ridge (Figs. 3, and 10c, "station" 4).

3.3.2 SAMW on 27.1–27.15

A significant difference between the western and eastern Pacific SAMWs is the spatial extent of the PV minimum. In

Fig. 9 Distribution of SAMW on the 27.05–γ^n surface. Details follow Fig. 4

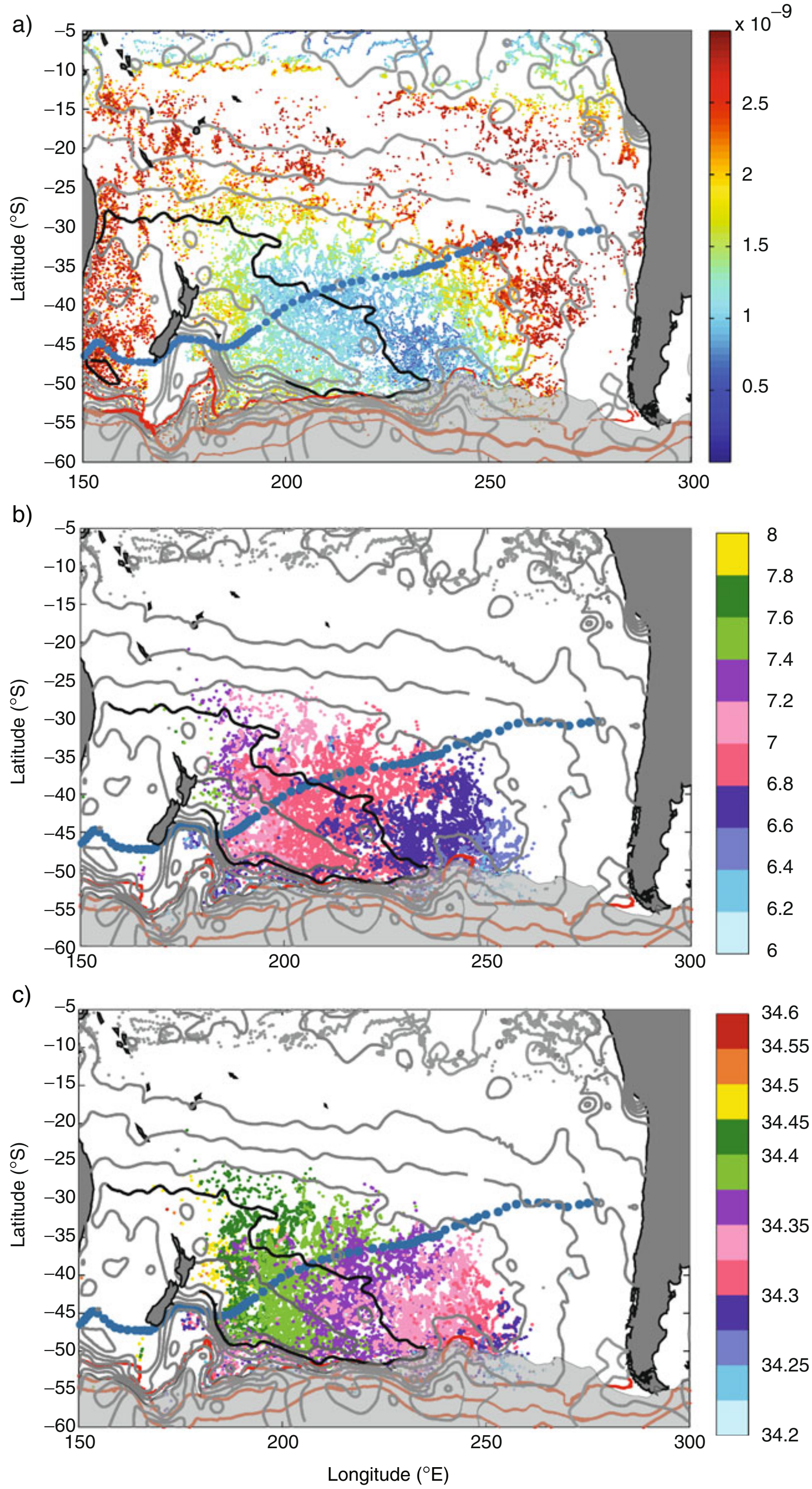

the west, the PV minimum is more intense but is limited in extent (e.g., the 27.05–γ^n SAMW); in the east, the PV minimum is less intense but of greater extent occupying the entire south Pacific Basin, with the exception of the Tasman Sea and near the South American coast. The eastern south Pacific Basin is occupied by the densest SAMW spanning a neutral density range of $27.1 \leq \gamma^n \leq 27.2$ kgm^{-3}. The lowest PV minima are found east of the East Pacific Rise (250° E) and west of the tip of South America (280° E; Figs. 11a and 12a). The spatial distribution of the PV minimum is again

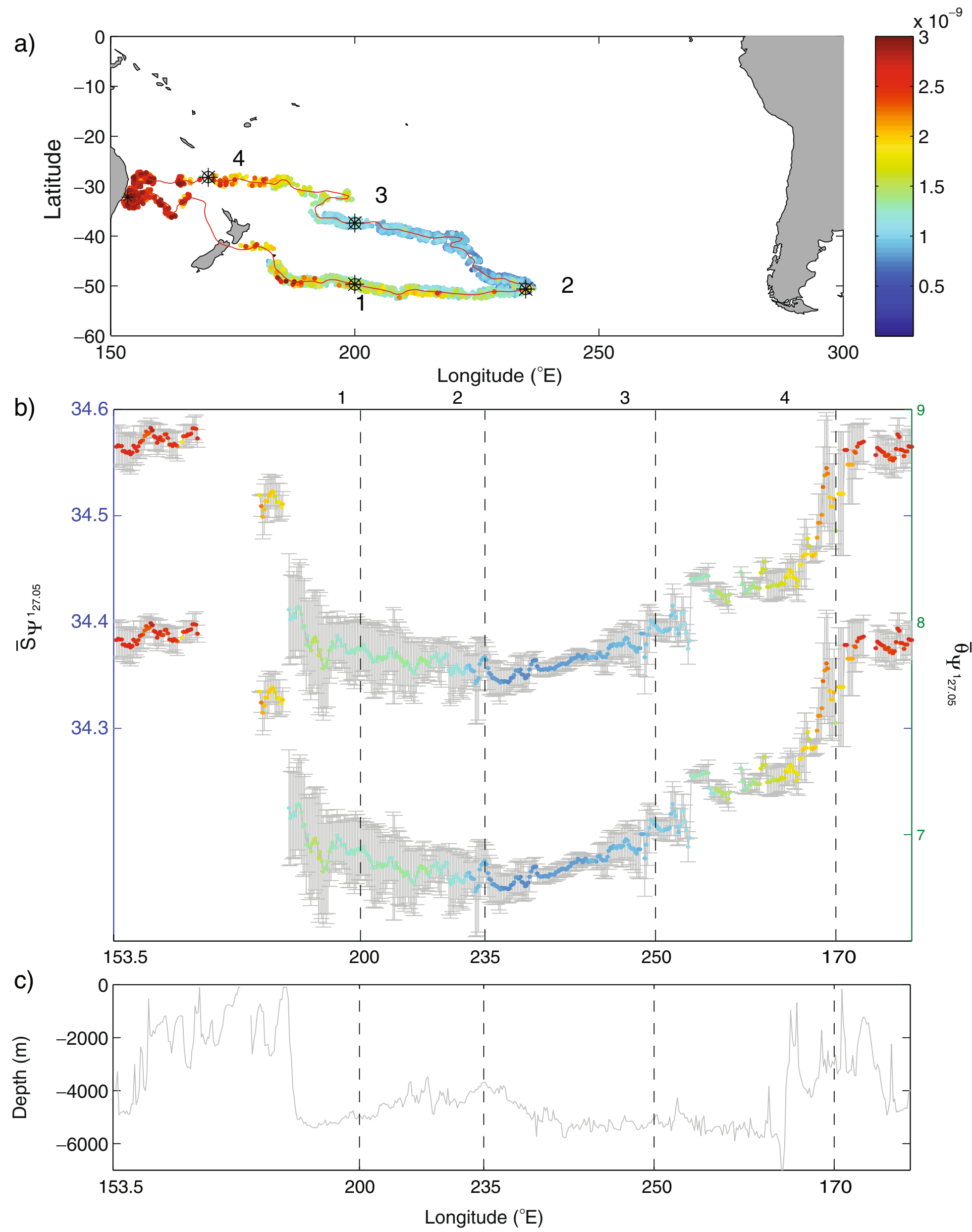

Fig. 10 Temperature and salinity changes along $\Psi_{27.05}$. **a** Colour-coded *dots* (according to the Potential vorticity) are Argo floats within 100 km from $\Psi_{27.05}$ (in *red*). *Black stars* where placed randomly to mark the eastward temperature and salinity anomaly changes along $\Psi_{27.05}$. **b** Temperature and salinity anomaly along $\Psi_{27.05}$. *Grey bars* denote the standard deviation. Each *dot* is the mean within a 100 km radius for every position in the streamline. Vertical *black dashed lines* indicate the position of the *black stars* in (**a**). **c** Ocean topography along $\Psi_{27.05}$

very distinctive on the neutral density surface on which it lies. For the 27.1–γ^n SAMW, low PV shows a similar pattern to that seen on the 27.05–γ^n surface but with the lowest PV cluster situated east of 250° E (Fig. 11a). A north- and northwest-ward circulation of the SAMW core can be inferred from the modified Montgomery streamlines in both neutral surfaces. The erosion of the pycnostad along streamlines is very low.

SAMW on the 27.1–γ^n surface occupies an extensive fan-like region of the central Pacific (50°–30° S, 210°–270° E) with temperature and salinity ranges of 6–6.4°C and 34.28–34.32, respectively (Fig. 11b, c). Once the PV minimum core starts eroding (~40° S, 230° E), temperature and salinity change rapidly when compared to the initial properties at the formation regions. A similar behaviour is found in the 27.15–γ^n surface (Fig. 12b, c). Properties of the SAMW core (5.2–5.6°C; 34.2–34.25) propagate northward up to 40°S along the $\Psi_{27.15}$ streamline (12; black bold line) at 270°–280° E from the formation region.

We have seen so far that temperature and salinity of the PV minimum increase as the PV minimum flows anti-clockwise from the Southern Ocean. Along the eastern side of the Tonga–Kermadec Rise (from ~45° S to 25° S at 190° E), warmer and saltier Tasman Sea waters mix with SAMW, rapidly changing its properties and eroding the PV minimum signature. This eastward flow is inferred from the increased temperature and salinity along ~35° S (between 190° and 200° E) and followed by the streamlines (also observed on previous density surfaces; Figs. 11 and 12). PV minimum waters with similar temperature and salinity values

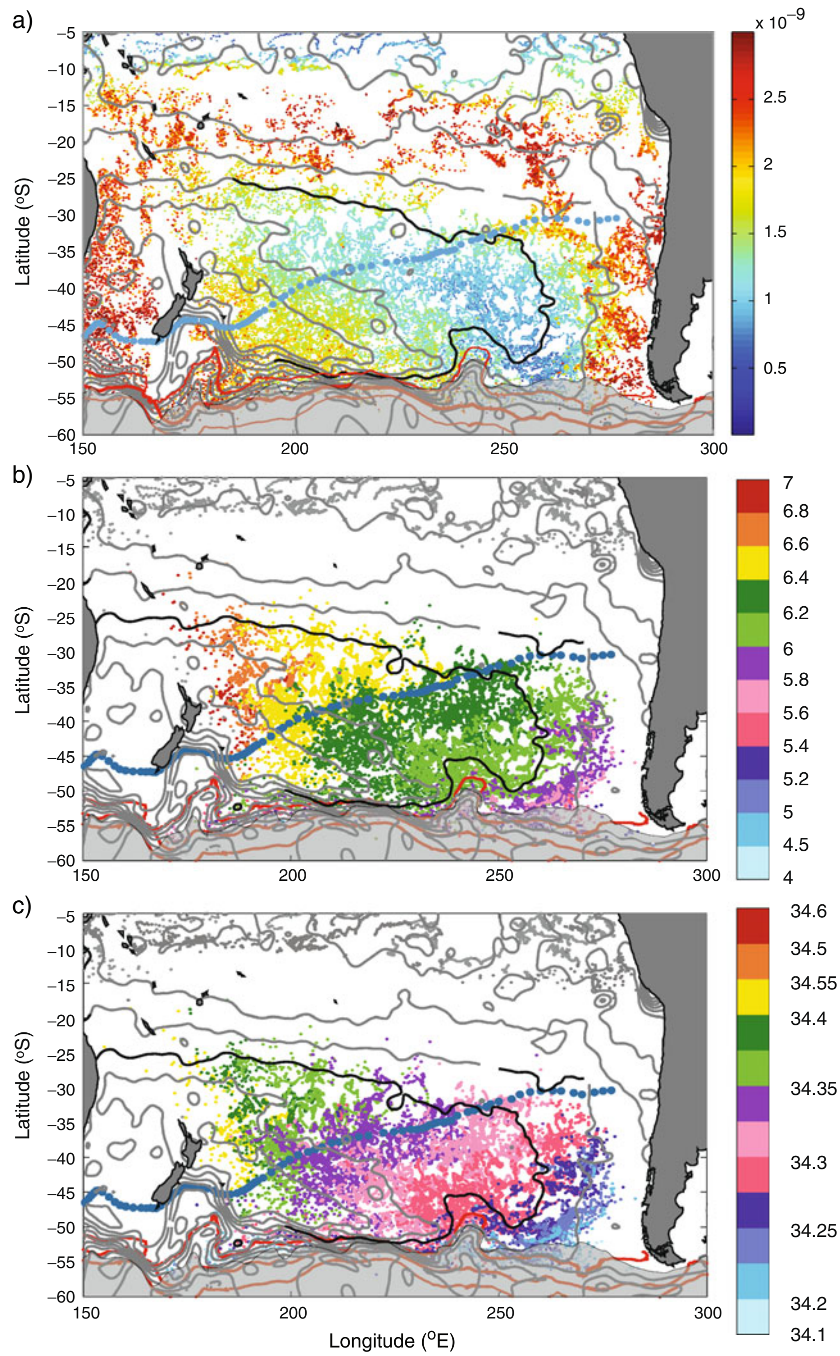

Fig. 11 Distribution of SAMW on the 27.1–γ^n surface. Details follow Fig. 4

to those in the southeast Pacific Ocean are also found in the SAF further west but are not exported to the subtropics at those longitudes.

3.4 SAMW in the South Atlantic Ocean

Contrary to the south Indian and south Pacific Oceans, there is no clear PV minimum "pool" associated with a specific density surface in the South Atlantic Ocean. However, weak modes are present in two γ^n ranges with links to SAMW properties, $26.5 \leq \gamma^n \leq 26.6$ and $27.15 \leq \gamma^n \leq 27.35$ kgm^{-3}. The lighter PV minimum layer is the south Atlantic Subtropical Mode Water defined in previous studies (e.g. McCartney 1977; 1982; Provost et al. 1995). This warm (14–15°C) and salty (~35.5) mode is limited to a narrow region of deep-mixed layers found north of the Brazil Current extention and, hence, is an example of a subtropical mode water. The denser PV minimum layer has two origins: (1) the southeast Ocean related to SAMW and (2) the equatorial atlantic. The latter has no connection to

Fig. 12 Distribution of SAMW on the 27.15–γ^n surface. Details follow Fig. 4

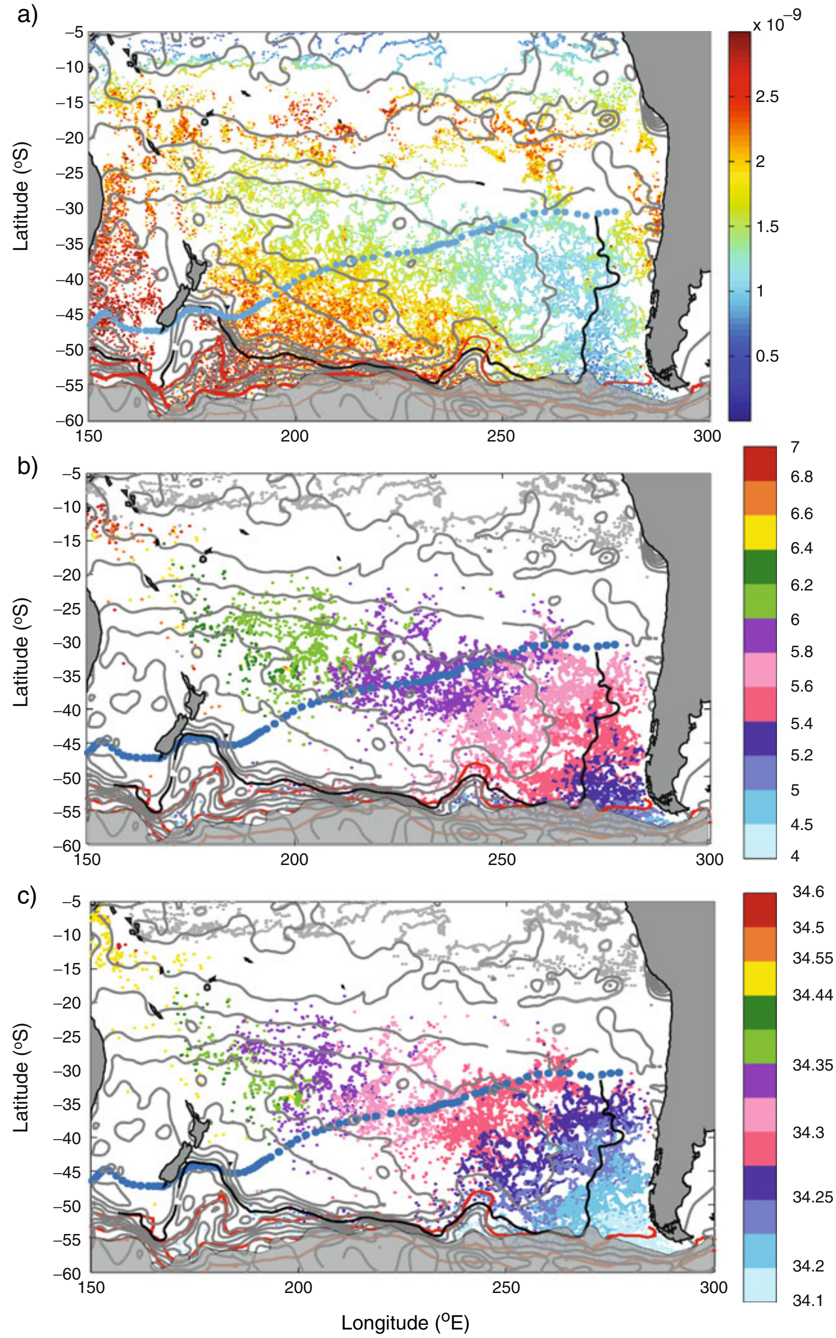

SAMW and spreads southward along the African coast in the Angolan Current (Stramma and England 1999; Lass and Mohrholz 2007).

Pacific SAMW entering the Atlantic through Drake Passage feeds into the salinity minimum layer, namely Antarctic Intermediate Water, as proposed by McCartney (1977). Figures 13 and 14 show a group of Argo floats used to explain the general state of the low PV layer in the South Atlantic. No distinction between seasons was made. The low PV layer occupies the upper 600–800 m as it flows eastward along Drake Passage. The PV minimum layer erodes faster at the shallower depths than at the lower ones as it moves eastward, being almost absent east of 30° W (not shown). The region between Drake Passage and the Brazil–Malvinas Confluence Zone (BMC) is not described due to lack of data. At the BMC, warm and salty waters of the Brazil Current occupy the top 200–400 m, below which the PV minimum coincides with the salinity minimum (Figs. 13 and 14, navy blue dots). East of the BMC, the low PV layer is less homogeneous and is seen as a patches centred at specific densities, γ^n=27.25, 27.3 and 27.35 kg m^{-3} (Figs. 13 and 14c), suggesting that AAIW with

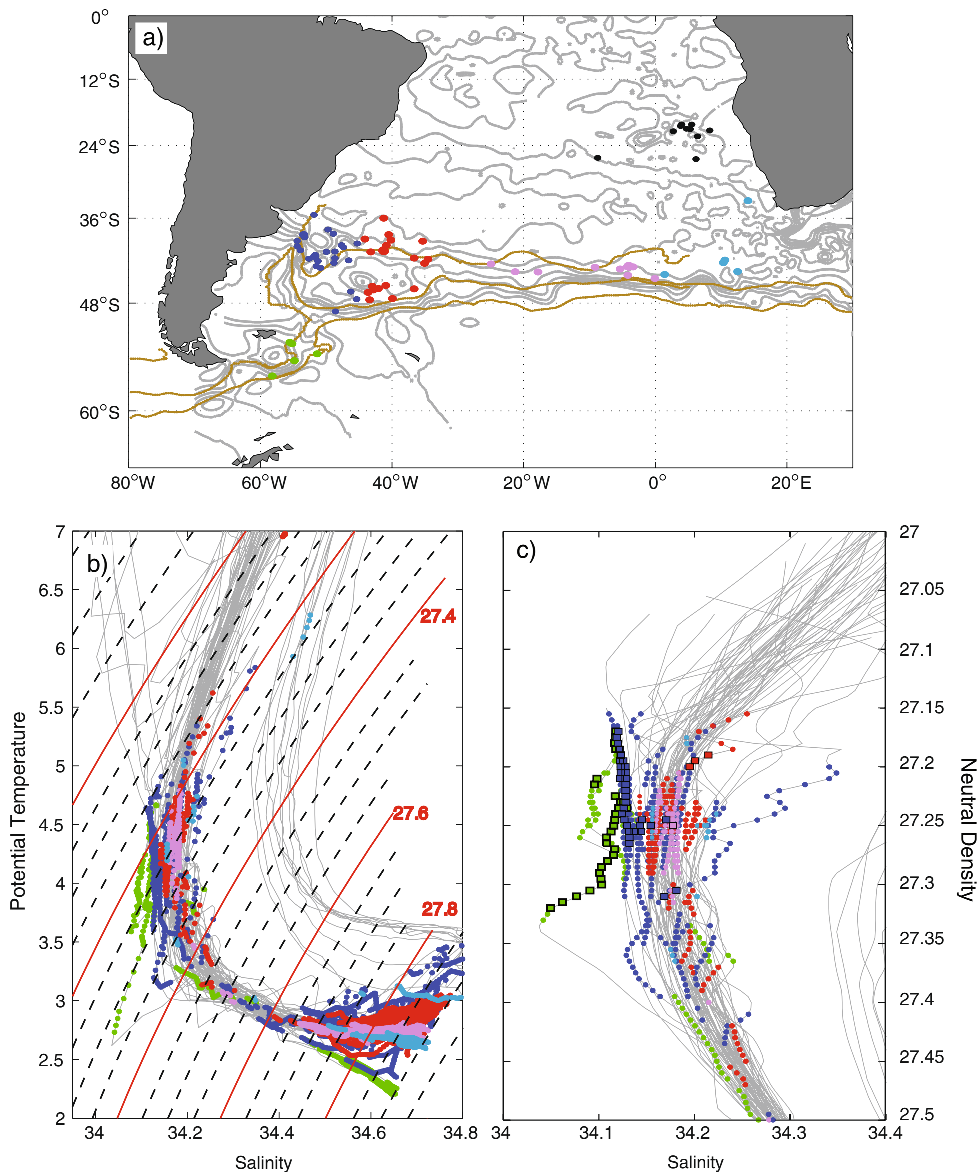

Fig. 13 Potential vorticity minima variability in the south Atlantic Ocean on the 27.25–γ^n surface. **a** Modified Montgomery streamlines at 27.25–γ^n surface. Argo floats are shown with a location colour-code: *green* ≤50° S; *navy blue* ≥50° S, ≤45° W; *red* ≥50° S, [45–30]° W; *pink* (30, 50] °S, [30, 0) °W; *light blue* [30, 50]° S, ≥0° W **b** Potential temperature—salinity relationship. **c** Salinity versus neutral density. *Dots* depict the portion of the profile where PV≤1.5×10^{-9} $m^{-1}s^{-1}$ and *squares*, where PV≤1×10^{-9} $m^{-1}s^{-1}$

different "history" recirculate back to the BMC through the South Atlantic Gyre, in agreement with the intermediate depth circulation suggested by Boebel et al. (1999). The salinity/PV minimum becomes warmer, saltier and higher in PV as it transits the basin (Figs. 13 and 14c).

3.5 Winter-mixed layer depth and volume of SAMW

Several physical mechanisms combine in the SAZ to enhance the formation and subduction of SAMW. The zero wind stress curl lies almost centred on the ACC circulation, north of which the Ekman layer converges and pumping occurs. Also, the rapid deepening of the isopycnals at the SAF preconditions the SAZ to the north to form deep-mixed layers. Finally, wintertime buoyancy loss from the ocean surface drives deep convection and the formation of mode waters in the Southern Ocean.

Deep-mixed layers and thick PV-minimum layers are found just north of the SAF, but the spatial distribution of both is patch-like rather than a continuous circumpolar feature. In the Indian Ocean, mixed layer depths deeper than 400 m are seen between 130° and 170° E. In the Pacific Ocean, two regions stand out as the deepest layers, separated from each other by the northern branch of the SAF (SAF-*n*) (Fig. 15a, red lines). The discontinuities seen in the circumpolar distribution of these two properties seem to coincide with changes in the neutral density at the base of the winter-mixed layer (Fig. 15). The fact that deep-mixed layers and thick low-PV layers coincide in space indicates that low-PV modes are exported to the north rather than advected to the east. Differences in deep-mixed layers of the Indian and Pacific oceans have also been related to differences in forcing mechanisms (Dong et al. 2008). Although this patchiness could also reflect Argo

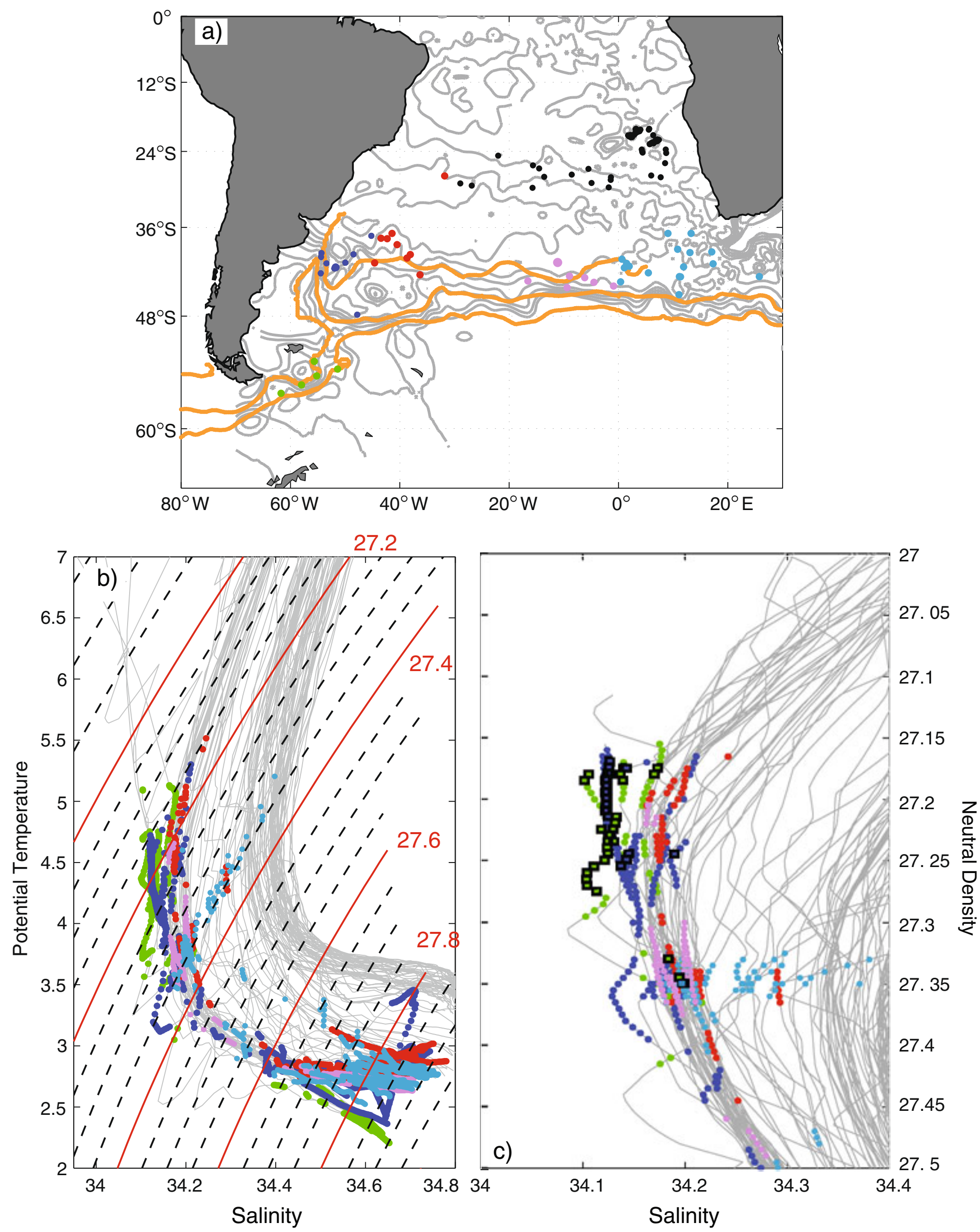

Fig. 14 Potential vorticity minima variability in the south Atlantic Ocean on the 27.35–γ^n surface. Details follow Fig. 13

sampling, we suggest that the discontinuities in the thickness of these two layers, both within each oceanic basin and circumpolarly, are related to large-scale circulation and mark the transition between types of SAMW and also subduction "hotspots" where SAMW enters the main thermocline.

SAMW modes are also distinguished in terms of their volume (Fig. 16). In the Indian Ocean, two modes are clearly distinguished at 26.8 and 26.9 kgm^{-3}, with the latter slightly more volumetric. In the Pacific Ocean, SAMW modes are not so clear; however the 27.05–γ^n SAMW mode shows up as the most volumetric mode. This mode also showed one of the strongest PV minimum layers. The Atlanctic Ocean shows no significant volumetric mode. These modes are likely to play an important role not only in ventilating the ocean interior but also in the transport of heat and freshwater. No significant volumetric mode was found for the salinity minimum layer.

4 Discussion

4.1 SAMW modes and circulation

The light mode waters in the south Atlantic have been described as either SAMW or Subtropical Mode Water (e.g. McCartney 1977; Maamaatuaiahutapu et al. 1994; Tsuchiya et al. 1994; Provost et al. 1995; De Miranda et al. 1999; Mémery et al. 2000). Identifying the boundary between waters north or south of the STF is complicated in the

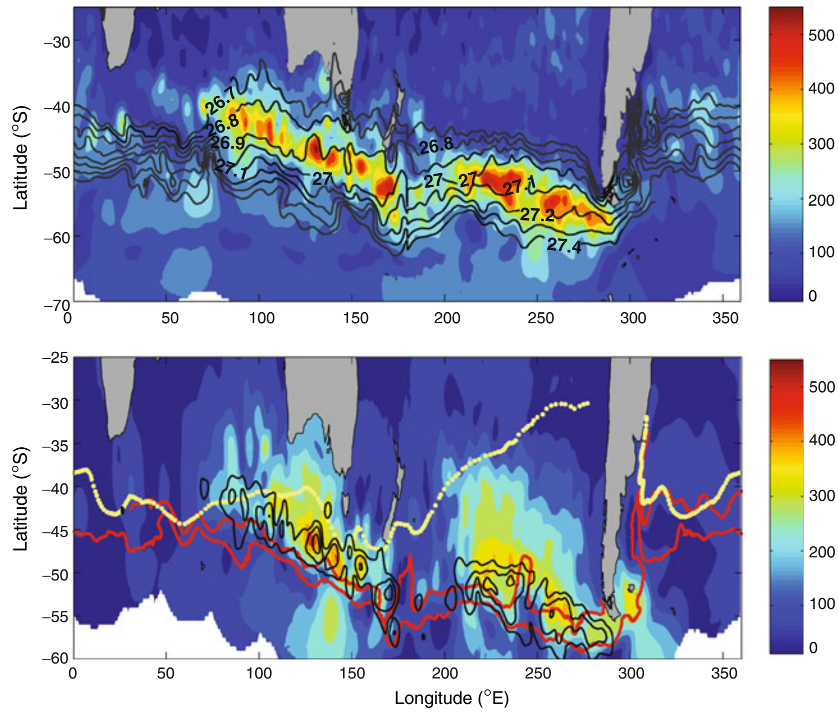

Fig. 15 **a** Mixed layer depth calculated following a density difference criterion with a threshold of 0.03 kgm^{-3} from Argo floats, during late winter conditions (September). **b** PV minimum thickness ($PV \leq 1 \times 10^{-9}\ m^{-1}s^{-1}$) during late winter conditions (September) plus the 300–400 m mixed layer depth location (*black lines*). *Yellow* and *red dot lines* show the location of the subtropical front and the subantarctic front. **a** and **b** has been mapped using a Loess fitting method (Ridgway et al. 2002). *Grey lines* depict the potential density at the base of the mixed layer

eddy-rich Brazil–Malvinas Confluence Zone. The lightest PV minimum waters ($26.5 \leq \gamma^n \leq 26.6$ kgm^{-3}) have a temperature of 14–16°C and a salinity of 34.5. This light mode is restricted to a very narrow region (30°–40° S, 30°–40° W). Strong eddy lateral mixing and stratification of the upper water column rapidly erode the PV minimum (Tsuchiya et al. 1994). Isolated profiles showed PV minimum signals east of the Brazil–Malvinas Confluence, probably flowing eastward by being trapped in long-lived mesoscale features as also suggested by Provost et al. (1995).

In the Indian Ocean, four types of SAMW are found with distinct circulation patterns, one more than identified in previous studies (McCartney 1982; Fine 1993; McCarthy and Talley 1999). McCartney (1982) pointed out the lighter SAMWs were confined to the southwest part of the subtropical gyre, in agreement with our observations. The 26.75–γ^n SAMW is found in a narrow region just west of the Southeast Indian Ridge, limited in the south by the SAF. An increase in the mixed layer depth east of the Southeast Indian Ridge marks the transition toward the 26.8–γ^n SAMW, extending from 80° to 100° E (Figs. 15a, and 17—see Section 4.1). Air–sea fluxes, eddy diffusion and northward Ekman transport are responsible for the preconditioning and formation of deep-mixed layers associated with SAMW east of 80° E (Sallèe et al. 2006). This SAMW type is confined between the Broken Plateau and the Southeast Indian Ridge (Fig. 17, purple). SAMW exported from this region forms a PV minimum extending north of 30° S and southeast of the Madagascar Basin.

Further east, between 100° and 120° E, the mixed layer depth increases, forming a SAMW with γ^n=26.8 kgm^{-3}. The PV minimum of the 26.8–γ^n SAMW can be traced from 50° S–120° E northwestward to 30° S–80° E, with little PV change (Fig. 17). Consequently, we conclude the subduction of SAMW in the SAZ southwest of Australia, between 100° and 120° E, to be highly effective in ventilating the ocean interior in agreement with previous studies (e.g., Fine 1993; Sallèe et al. 2010). This SAMW class can be followed up to 20° S, east of Madagascar Island, before it is completely mixed (i.e. the low PV layer is eroded).

South of Australia, the $26.9 \leq \gamma^n < 27$ SAMW constitutes the largest volumetric class of SAMW in the south Indian Ocean (Fig. 16). The core of the 26.9–γ^n SAMW is located north of the SAF at ~110° E (Fig. 5a). It is in this region where two SAMWs coexist (26.8–γ^n and 26.9–γ^n SAMW) and subduct to form part of the lower thermocline and feed Indian Central Water (You and Tomczak 1993). Although they subduct in similar regions, they follow different export paths. While the lighter SAMW enters the subtropical gyre following a northwestward geostrophic flow, the denser SAMW is forced to follow two routes as it encounters the Broken Plateau (Fig. 17). The influence of the Broken Plateau is highlighted by the fact that very few Argo profiles are found north/northwest of the Plateau. This encounter of the flow with the Broken Plateau likely enhances mixing, inferred from the sudden change in PV (and temperature and salinity) seen along streamlines in this location (Fig. 6).

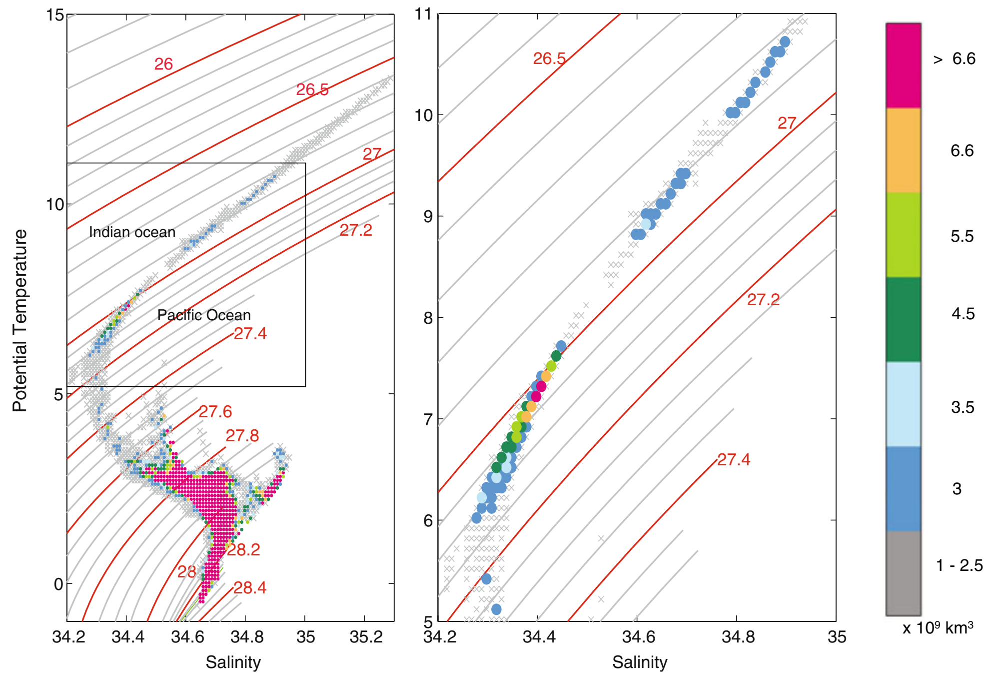

Fig. 16 CARS2009 volumetric temperature (T) and salinity (S) in 0.1° and 0.01 T and S class. **a** CARS T/S class in the southern hemisphere. **b** SAMW T/S class (*black square* in (**a**)). Each *dot* represents a T/S class with a volume colour-code. Only large volume (>10^9 km^3) modes are shown. *Grey* and *red* contours in the background depict neutral density isopycnals

Two northwestward flows describe the export of SAMW on the 26.9–γ^n surface: (1) SAMW joins the subtropical gyre west of the Broken Plateau; (2) SAMW first flows northward along the western Australian coast to ~20° S, where SAMW flows northwestward. Reid (2003) used World Ocean Circulation Experiment sections to map the large-scale geostrophic flow in the Indian Ocean at various depths. He inferred poleward flow along the western coast of Australian at depths from 0 to 3,000 dbar. Our observations, on the other hand, suggest an equatorward flow along the western Australian Coast. Domingues et al. (2007) proposed a new 3-D view of the upper-circulation of the Southeastern Indian Ocean in which the net anticyclonic movement of the Subtropical Gyre is, in fact, formed by a combination of dominant zonal flows—a latitudinal succession of near surface eastward jets and deeper westward jets—linked with the equatorward boundary flow of the Leeuwin Undercurrent, along the west Australian continental slope. Near Cape Leeuwin (35° S), the Leeuwin Undercurrent transports South Indian Central Water, SAMW and AAIW. Only a small fraction of the deeper water masses, SAMW and AAIW, remains "coastally-trapped" and is advected towards lower latitudes by the Leeuwin Undercurrent (Domingues et al. 2007). These zonal flows are also clear in the vertical distribution of oxygen,[3] in which two clusters of high oxygen are found at 30°–25° S and at ~20° S, where SAMW flows westward (not shown).

[3] Oxygen data corresponds to the World Ocean Circulation Experiment (WOCE) section I08N.

The strongest PV minimum associated with SAMW is found on the 26.94–γ^n surface in the Great Australian Bight (Fig. 7). As observed in Section 3.3.1, a strong PV minimum signal extends from 120° E to south of Tasmania. SAMW likely subducts south of Tasmania but it is between 100°–120° E that it gets exported into the subtropical gyre following a similar route as the 26.9–γ^n SAMW (Fig. 5). This SAMW type is also found east and west of New Zealand. Temperature and salinity ranges are of similar magnitude in both SAMW clusters, suggesting that these two clusters are formed locally under similar forcing rather than downstream evolution of properties (at least at the 26.94–γ^n surface). West of New Zealand, the SAMW is warmer and saltier in the northern side of the Subantarctic Zone due to the strong subtropical influence over the SAZ, east/southeast Tasmania (Herraiz-Borreguero and Rintoul 2010).

A shift in the neutral density range of the low PV SAMW toward denser modes characterises the south Pacific Ocean SAMWs (Fig. 16). In previous studies, the lightest Pacific SAMWs were shown to be limited to the western Pacific (the Tasman Sea and east of New Zealand), while the densest SAMWs were found in the southeast Pacific (McCartney and Baringer 1993; Sokolov and Rintoul 2000). Two branches had been suggested to account for the circulation of densest SAMWs formed east of the South Pacific Rise. The northern branch spreads northwestward with the outer subtropical gyre and enters the Coral Sea north of Vanuatu (Sokolov and Rintoul 2000). The southern branch was inferred by McCartney and Baringer (1993), and it is limited to south of 35° S. Here,

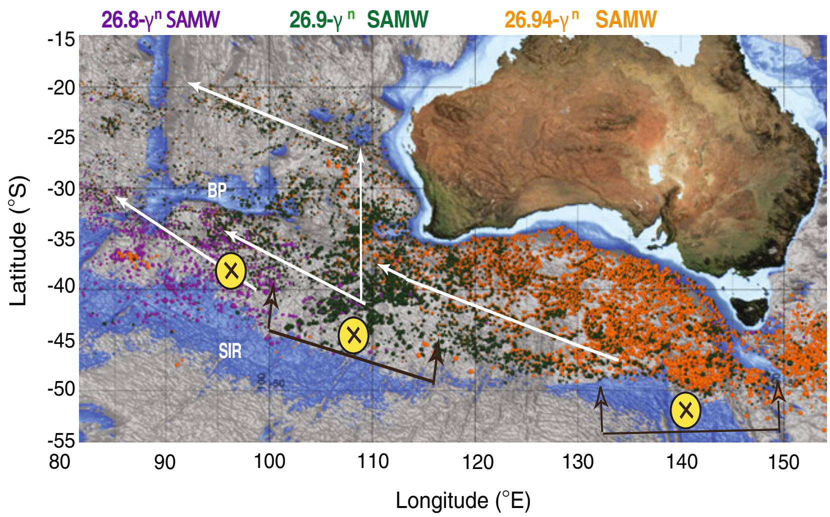

Fig. 17 South Indian Ocean SAMW types and circulation (*white arrows*). From east to west: 26.8–γ^n (*purple*), 26.9–γ^n (*green*), and 26.94–γ^n (*orange*) SAMW types. *Yellow circles* show schematically regions where SAMW subduction occurs. The size of the dots is inversely proportional to the PV minimum value. Main bathymetry is in blue. *BP* broken plateau, *SIR* South Indian Ridge

we propose a variant for this two-branch circulation in which the SAMW circulation follows three routes in the South Pacific and a fourth path through Drake Passage.

Route 1 The lightest (γ^n=27.0 kgm^{-3}) of the South Pacific SAMW is found east of New Zealand (Figs. 8 and 18b, blue dots). Deep-mixed layers (ML) are first developed east of 220° E, with a neutral density of 27.0 kgm^{-3} at the base of the ML coincident in space (50°–55° S and 220° E) with the 27.0–γ^n SAMW core (Fig. 15). The Montgomery streamlines and 27.0–γ^n properties suggest a nearly closed recirculation east of New Zealand, leaving this type of SAMW restricted to the centre of the subtropical gyre (Fig. 8). Also, warmer and saltier 27.0–γ^n SAMW (compared to the properties just north of the SAF), with higher potential vorticity values and low oxygen concentrations,[4] turns poleward into the gyre completing the recirculation, east of New Zealand (Fig. 8b, c).

Route 2 The south western Pacific Basin is dominated by the 27.05–γ^n SAMW (Fig. 18a, green dots). It resembles the circulation pattern of the 27.0–γ^n SAMW but with a broader zonal and meridional extent. The most prominent feature of the 27.05–γ^n SAMW is the strong PV minimum signal associated with the core of the mode water (Fig. 9). The large northwestward extension of the SAMW core suggests a very efficient export of 27.05–γ^n SAMW into the subtropical gyre, likely subducting north of the SAF at 240° E, in agreement with Sallèe et al. (2010). The export of the 27.05–γ^n SAMW corresponds to the southern branch described in previous works (McCartney and Baringer 1993; Sokolov and Rintoul 2000), although we show the origin of this mode to be in the western–central Pacific rather than the result of a diversion of flow of the denser SAMWs from the southeastern Pacific. An oxygen maximum layer associated with a PV minimum was identified at a neutral density level of 27.1–27.2 kgm^{-3} along 32° S (Wijffels et al. 2001), supporting our claim that the lighter south Pacific SAMWs do not extend as far north as 30° S (Figs. 11, 12 and 17).

The 27.1–γ^n SAMW core spreads northward from north of the SAF to just south of 40° S before it turns northwestward (Fig. 18b, green dots). This path resembles the one followed by the 27.05–γ^n SAMW although the relatively denser SAMW reaches further north and west. Thus, the ventilation of the south and, especially, the low latitude Pacific depends mainly on the formation and circulation of the 27.1–γ^n SAMW.

Route 3 The last of the circulation paths of the Pacific SAMW occurs along the outer rim of the subtropical gyre. The PV minimum core at γ^n=27.15 kgm^{-3} spreads northward from the formation region near 55° S between 270° and 280° E. The flow turns westward at approximately 25° S. This northward flow resembles the export path of AAIW described by Iudicone et al. (2007), in which AAIW is injected in the subtropical gyre east of 90° W.

The southeastern SAMWs appear to join the South Equatorial Current in its westward flow. Geostrophic circulation maps at 500 and 800 dbar (Reid 1997) show a westward circulation between 15° and 25° S, consistent with the inferred circulation of the (27.1–27.15)–γ^n SAMW. The South Equatorial Current splits into jets when it encounters the complex topography of the southwest Pacific (Sokolov and Rintoul 2000). Part of the eastern SAMW flows cyclonically round the Gulf of Papua New Guinea to ultimately enter the Solomon Sea. The remaining SAMW turns southward feeding the East Australian

[4] Oxygen concentrations obtained from the Southern Ocean Data Base, http://wocesoatlas.tamu.edu/Sites/html/atlas/SOA_DATABASE.html.

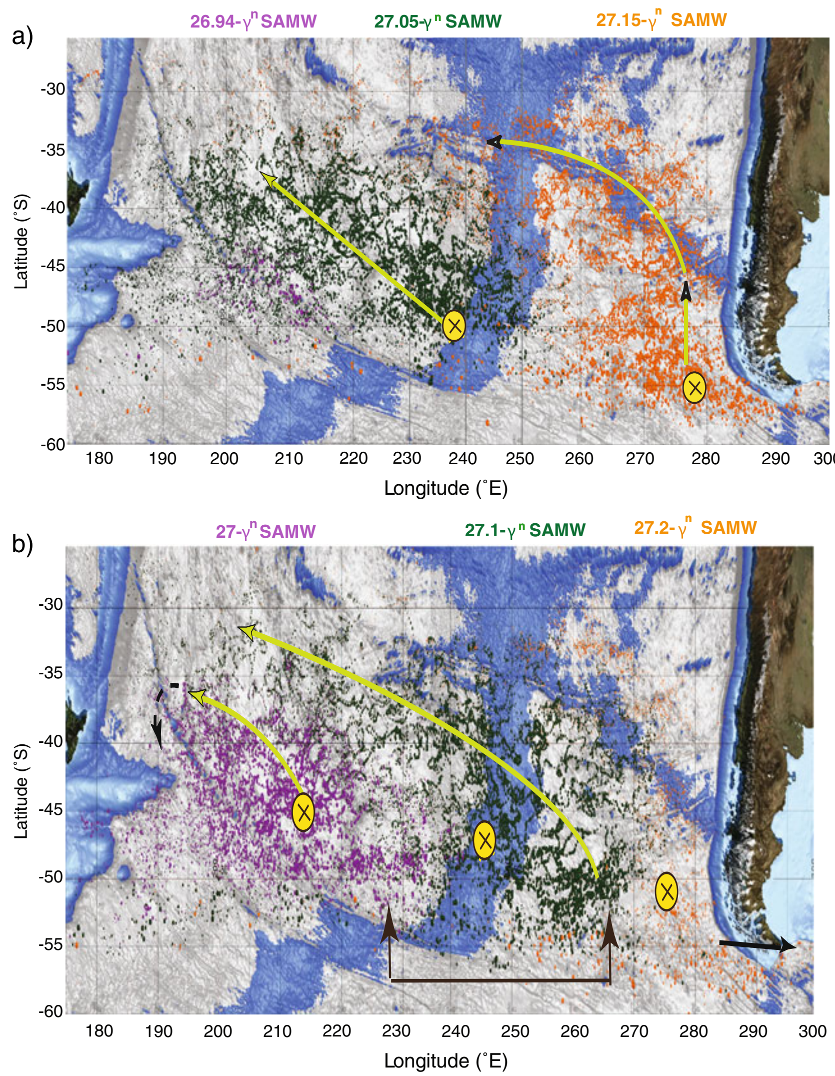

Fig. 18 South Pacific Ocean SAMW types and circulation (*green arrows*). SW and SE Pacific SAMW types, from east to west: 26.94–γ^n (*purple*), 27.05–γ^n (*green*), and 27.15–γ^n (*orange*) SAMW types (**a**). SW and SE Pacific SAMW types, from east to west: 27–γ^n (*purple*), 27.1–γ^n (*green*), and 27.2–γ^n (*orange*) SAMW types. (**b**). *Yellow circles* show schematically regions where SAMW subduction occurs. The size of the *dots* is inversely proportional to the PV minimum value. Main bathymetry is in *blue*

Current (Sokolov and Rintoul 2000). In our PV minimum map at 27.1–γ^n and 27.15–γ^n surfaces (Figs. 11a and 12a), the PV minimum gets eroded very fast due to the vigorous stirring of the eddy field that homogenises temperature and salinity along isopycnals west of the Tonga–Kermadec Ridge (Sokolov and Rintoul 2000).

Route 4 Several studies have agreed that SAMW is a precursor for the formation of AAIW (e.g. McCartney 1977; Talley 1996). However, Naveira-Garabato et al. (2009) claimed that the inter–annual variability of the southeastern Pacific AAIW properties is primarily driven by changes in AASW properties rather than SAMW variability. In the South Atlantic, on the other hand, there is an overall agreement that the densest SAMW contributes to AAIW formation, after SAMW enters Drake Passage. Naviera-Garabato et al. (2003) applied an inverse model along the rim of the Scotia Sea. The surplus of AAIW/AASW exported from the Scotia Sea by the ACC was suggested to be due in part to conversion of SAMW to AAIW, by mixing processes (effective diffusion) in the upper ocean. By following the PV minimum signature of SAMW into the south Atlantic Ocean, the conversion of the SAMW into a salinity minimum layer could be followed (Section 3.3, Figs. 13 and 14), with the exception of the Malvinas Current which is not represented (as yet) by Argo data. Our results confirm that the upper part of the salinity minimum layer in the south Atlantic Ocean is supplied by the potential vorticity minimum imported from the south Pacific Ocean.

4.2 SAMW subduction

SAMW subduction shows high regional variability circum-polarly and occurs in “hotspots”. The subduction/ventilation of mode and intermediate waters has been of great interest since the 1990s as they ventilate the permanent thermocline in regions distant from their formation areas in the Southern Ocean. The locations where SAMW modes subduct inferred from the PV minimum distribution are schematically shown in Figs. 17 and 18. In the South Indian Ocean, the spread of the PV–minimum layer from the Southern Ocean to the subtropical gyre occurs in two regions (90°–110° E; and, south of Tasmania 130°–160° E) at the 26.8–γ^n and 26.9–γ^n surfaces, respectively (Fig. 17, yellow circles). In the south Pacific Basin, SAMW modes subduct east of New Zealand (~210° E), east and west of the Southeast Pacific Ridge (centred at ~250° E), and west of Drake Passage (~270°–280° E).

SAMW subduction "hotspots" are consistent with some of the subduction regions defined by Sallée et al. (2010). Sallèe et al. (2010) calculated subdution from a mass budget through the base of the winter-mixed layer. Their analysis did not capture all regions where subduction f SAMW has been inferred CFC and tracers studies (below). This might be explained by the strong dependence on the climatologically mixed layer used. These regions are south of Tasmania (Figs. 7 and 17), and especially, the southeast Pacific (Figs. 12 and 18). Also, discrepancies are observed when comparing the subduction/upwelling estimates with PV distributions on density surfaces (their Fig. 11). A finer density criteria to calculate the subduction rates might explain some of the observed discrepancies.

Our results agree with SAMW subduction regions previously inferred from CFC analysis. In the southeast Indian Ocean, the strongest PV minimum signatures are related to the denser types of SAMW ($26.9 \leq \gamma^n \leq 26.95$ kg m^{-3}). Our results agree with the location of a layer of young SAMW (approximately 5 years old) by Karstensen and Tomczak (1997). High CFC concentrations observed in the southeast Indian Ocean indicate this region as the source for recently ventilated thermocline water entering the north Indian Ocean mainly through the eastern Indian Ocean (e.g., Wyrtki 1971; Stramma and Lutjeharms 1997; Fine et al. 2008; Sloyan and Rintoul 2001). Fine et al. (2008) highlighted the differences between the southwest and southeast SAMWs regarding their CFC concentrations and ages. The SE SAMW was lower in PV, higher in CFCs, denser (γ^n=26.8 kgm^{-3}), and younger (2–4 years) than the SW SAMW (γ^n=26.6 kgm^{-3}, ~14 years). The lack of data did not allow CFC ages to be calculated for the 26.9–γ^n SAMW mode south of Australia. In the Pacific Ocean, SAMW occupies a vast area of the south Pacific with a considerable export at several locations, each reaching different subtropical gyre regimes. Either side of the East Pacific Rise (Fig. 3) and in the southeast Pacific, a tongue of low PV at two density levels (γ^n=27.05 kgm^{-3} and γ^n= 27.1 kgm^{-3}) suggests this site to be important in exporting SAMW into the gyre (Figs. 9 and 11) and, hence, in ventilating the subtropical gyre (e.g. Fine et al. 2001; Hartin et al. 2010, in preparation).

A complete analysis on SAMW subduction is given by, for instance, Talley (1999), You (1998), Fine et al. (2001, 2008), Karstensen and Quadfasel (2002a, b), Qu et al. (2008), and Sallèe et al. (2010).

5 Conclusions

The broad-scale, year-round sampling of the southern hemisphere oceans by Argo profiling floats allows the formation regions and circulation pathways of SAMW to be mapped in unprecedented detail. In particular, the new observations reveal that the SAMW consists of a set of distinct modes, each with a characteristic density, formed in particular locations, subducted through narrow ventilation windows and that follow well-defined pathways into the ocean interior.

The circulation of lighter modes formed in the western and central parts of the Indian and Pacific basins is limited to the southwest portion of the subtropical gyres. Denser modes formed in the southeastern part of the basin are carried further north by the outer portion of the subtropical gyre and ventilate a larger fraction of the gyre interior. Relative to the other ocean basins, the Atlantic is characterised by shallow-mixed layers and a small volume of mode water. Low potential vorticity mode water imported from the Pacific supplies the salinity minimum layer of the AAIW in the Atlantic, as suggested by earlier studies.

The circulation pathways are influenced strongly by bathymetry. Bathymetric features are also associated with rapid transitions in mode water properties, supporting the hypothesis that mixing is enhanced near significant sea floor topography, even at intermediate depths. In contrast, over the deep basins and smooth topography, the mode water properties are nearly conserved over long distances, suggesting very little mixing takes place there.

The subduction "hotspots" inferred from the interior distribution of potential vorticity, temperature and salinity agree well with those inferred from an independent analysis of the mass balance above the depth of the winter-mixed layer (Sallèe et al. 2010) and CFC analysis. Our results suggest that the west-to-east evolution of SAMW properties towards cooler, fresher and denser modes is the result of the formation and export of distinct mode water varieties in these "hotspots," rather than the gradual, continuous modification by air–sea fluxes as originally proposed based on the sparse observations available in the 1970s.

References

Barker PJ, Dunn R, Wijffels SE and Domingues CM (2010). Pressure sensor drifts in Argo and their impacts. J Tech Ocean Atmos, in press

Boebel O, Davis RE, Ollitrault M, Peterson RG, Richardson PL, Schmid C, Zenk W (1999) The intermediate depth circualtion of the Western South Atlantic. Geophys Res Lett 26(21):3329–3332. doi:0094-8276/99/1999GL002355

De Miranda AP, Barnier B, Dewar WK (1999) Mode waters and subduction rates in a high–resolution South Atlantic simulation. J Mar Res 57:213–244

Domingues CM, Maltrud ME, Wijffels SE, Church JA, Tomczak M (2007) Simulated Lagrangian pathways between the Leeuwin current system and the upper–ocean circulation of the southeast Indian Ocean. Deep-Sea Res II (Special Issue) 54(8–10):797–817. doi:10.1016/j.dsr2.2006.10.003

Dong S, Sprintall J, Gille ST, Talley L (2008) Southern Ocean mixed–layer depth from Argo float profiles. J Geophys Res 113:C06013. doi:10.1029/2006JC004051

Dunn JR, Ridgway KR (2002) Mapping ocean properties in regions of complex topography. Deep Sea Res I 49:591–604

Fine RA (1993) Circulation and antarctic intermediate water in the South Indian Ocean. Deep Sea Res 40:2021–2042

Fine RA, Maillet KA, Sullivan KF, Willey D (2001) Circulation and ventilation of the Pacific Ocean. J Geophys Res 106 (C10):22159–22178

Fine RA, Smethie WM Jr, Bullister JL, Rhein M, Min D-H, Warner MJ, Poisson A, Weiss RF (2008) Decadal ventilation and mxing of Indian ocean waters. Deep Sea Res I 55:20–37

Hanawa K, Talley LD (2001) Mode waters. In: Siedler G, Church J, Gould J (eds) Ocean circulation and climate, international geophysics series. Academic, New York, pp 373–386

Herraiz-Borreguero L, and Rintoul SR (2010) Regional circulation and its impact on upper ocean variability south of Tasmania (Australia). Deep-Sea Research II—Antarctic Biogeochemistry special edition, in press.

Iudicone D, Rodgers KB, Schopp R, Madec G (2007) An exchange window for the injection of Antarctic intermediate water into the South Pacific. J Phys Oceanogr 37:31–49. doi:10.1175/JPO2985.1

Jackett DR, McDougall TJ (1997) A neutral density variable for the world's oceans. J Phys Oceanogr 27:237–263. doi:10.1175/1520-0485(1997)027

Karstensen J, Quadfasel D (2002a) Formation of southern hemisphere thermocline waters: water mass conversion and subduction. J Phys Oceanogr 32:3020–3038

Karstensen J, Quadfasel D (2002b) Water subducted into the Indian Ocean subtropical gyre. Deep Sea Res II 49:1441–1457

Karstensen J, Tomczak M (1997) Ventilation processes and water mass ages in thermocline of the southeast Indian Ocean. Geophys Res Lett 24:2777–2780

Lass HU, Mohrholz V (2007) On the interaction between the subtropical gyre and the subtropical cell on the shelf of the SE Atlantic. J Mar Res 74:1–43

Maamaatuaiahutapu K, Provost C, Andrié C, Vigan X (1994) Origin and ages of mode waters in the Brazil–Malvinas confluence region during austral winter 1994. J Geophys Res 104 (C9):21051–21061

McCarthy M, Talley LD (1999) Three–dimensional isonetral potential vorticity structure in the Indian Ocean. J Geophys Res 104 (C6):13251–13267

McCartney MS (1977) In: Angel M (ed) Subantarctic mode water. In a voyage of discovery, supplement to deep–sea research George Deacon 70th anniversary volume. Pergamon, New York, pp 103–119

McCartney MS (1982) The subtropical recirculation of mode waters. J Mar Res 40(Suppl):427–464

McCartney MS, and Baringer MO (1993) Notes on the S. Pacific hydrographic section near 32 °S—WHP P. WOCE Notes, 5.

McDougal TJ, Klocker A (2010) An approximate geostrophic streamfunction for use in density surfaces. Ocean Model 32:105–117

McDougall TJ (1989) Streamfunctions for the lateral velocity vector in a compressible ocean. J Mar Res 47:267–284

Mémery L, Arhan M, Alvarez-Salgado XA, M-J Messias, Mercier H, Castro GC, Rios AF (2000) The water masses along the western boundary of the south and equatorial Atlantic. Prog Oceanogr 47:69–98

Montgomery RB (1937) A suggested method for representing gradient flow in isentropic surfaces. Bull Am Meteorol Soc 18:210–212

Naveira-Garabato AC, Jullion L, Stevens DP, Heywood KJ, King BA (2009) Variability of subantarctic mode water and antarctic intermediate water in Drake passage during the late 20th and early 21 st. centuries. J Clim 22(13):3361–3388. doi:10.1175/2009JCLI2621.1

Naviera-Garabato AC, Stevens DP, Heywood KJ (2003) Water mass conversion, fluxes, and mixing in the Scotia Sea diagnosed by an inverse model. J Phys Oceaongr 33:2565–2568

Provost C, Gana S, Garçon V, Maamaatuaiahutapu K, England M (1995) Hydrographic conditions in the Brazil–Mavinas confluence during austral summer 1990. J Geophys Res 110 (C6):10655–10678

Qu T, Gao S, Fukumori I, Fine RA, Lindstrom EJ (2008) Subduction of South Pacific waters. Geophys Res Lett 35:L02610. doi:10.1029/2007GL032605

Reid JL (1997) On the total geostrophic circulation of the Pacific Ocean: flow patterns, tracers, and transports. Prog Oceanogr 39:263–352

Reid JL (2003) On the geostrophic circulation of the Indian Ocean: flow patterns, tracers, and transports. Prog Oceanogr 56:137–186

Ridgway KR, Dunn JR, Wilkin JL (2002) Ocean interpolation by four-dimensional least squares–application to the waters around Australia. J Atmos Ocean Technol 19(9):1357–1375

Rintoul SR, England MH (2002) Ekman transport dominates local air-sea fluxes in driving variability of subantarctic mode water. J Phys Oceanogr 32:1308–1321

Roden G (1986) Thermohaline fronts and baroclinic flow in the Argentine basin during the austral spring of 1984. J Geophys Res 91:5075–5093

Sallèe JB, Wienders N, Morrow R, Speer K (2006) Formation of subantarctic mode water in the Southeastern Indian Ocean. Ocean Dyn 56:525–542

Sallèe JB, Morrow R, Speer K (2008) Eddy heat diffusion and subantarctic mode water formation. Geophys Res Lett 35: L05607

Sallèe JB, Speer K, Rintoul SR, Wijffels S (2010) Southern Ocean thermocline ventilation. J Phys Oceanogr 40(3):509–529

Scharffenberg MG, Stammer D (2010) Seasonal variations of the large-scale geostrophic flow field and eddy kinetic energy inferred from the TOPEX/Poseidon and Jason-1 tandem mission data. J Geophys Res 115:C02008. doi:10.1029/2008JC005242,2010

Sloyan B, Rintoul SR (2001) Circulation, renewal and modification of Antarctic mode and intermediate water. J Phys Oceanogr 31:1005–1030

Sokolov S, Rintoul SR (2000) Circulation and water masses along WOCE section P11: Papua New Guinea to Tasmania. J Mar Res 58:223–268

Stramma L, England M (1999) On the water masses and mean circulation of the South Atlantic Ocean. J Geophys Res 104(C9):20863–20883

Stramma L, Lutjeharms JRE (1997) The flow field of the subtropical gyre of the South Indian Ocean. J Geophys Res 102(C3):5513–5530

Talley LD (1996) Antarctic intermediate water in the South Atlantic. In: Wefer G, Berger WH, Siedler G, Webb DJ (eds) The South Atlantic: present and past circulation. Springer, New York, pp 219–238

Talley LD (1999) Some aspects of ocean heat transport by the shallow, intermediate and deep overturning circulations. Mechanisms of global climate change at millennial time scales. Geophys Monogr 112:1–22

Tsuchiya M, Talley LD, McCartney MS (1994) Water–mass distributions in the western South Atlantic; a section from the South Georgia Island (54 S) northward across the equator. J Mar Res 52:55–81

Wijffels SE, Toole JM, Davis R (2001) Revisiting the South Pacific subtropical circulation: a synthesis of the world ocean circulation experiment observations along 32 °S. J Geophys Res 106 (C9):19481–19513

Wyrtki K (1971) Oceanographic Atlas of the international Indian Ocean expedition. National Science Foundation, Washington DC, p 531

You Y (1998) Intermediate water circulation and ventilation in the Indian Ocean derived from water-mass contributions. J Mar Res 56:1029–1067

You Y, Tomczak M (1993) Thermocline circulation and ventilation in the Indian Ocean derived from water mass analysis. Deep Sea Res 40:13–56

Zhang H-M, Hogg NG (1992) Circulation and water mass balance in the Brazil Basin. J Mar Res 50:385–420